Ecological Indicators 150 (2023) 110262

Contents lists available at ScienceDirect

Ecological Indicators

journal homepage: www.elsevier.com/locate/ecolind

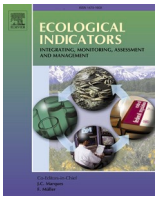

Developing global annual land surface phenology datasets (1982–2018) from the AVHRR data using multiple phenology retrieval methods

Wei Wu [a], Ziming Li [b], Zhicheng Zhang [a], Chenxi Yan [c], Kun Xiao [a], Yidan Wang [a], Qinchuan Xin [a,*]

[a] School of Geography and Planning, Sun Yat-sen University, Guangzhou, China
[b] Division of Landscape Architecture, Faculty of Architecture, The University of Hong Kong, Hong Kong, China
[c] School of Atmospheric Sciences, Sun Yat-sen University, Guangzhou, China

ARTICLE INFO

Keywords:
Land surface phenology
Vegetation growing seasons
Satellite product
Remote sensing
Time series

ABSTRACT

Land surface phenology that reflects periodical changes in terrestrial vegetation plays an important role in influencing the functioning and services of ecosystems. Satellite-derived metrics of land surface phenology have been widely used to assess the patterns in land cover dynamics. There are still limited satellite-based datasets of global land surface phenology available to date due to uneven qualities of satellite data. Here, we developed a global annual land surface phenology dataset based on Advanced Very High Resolution Radiometer (AVHRR) data from 1982 to 2018. The number of global vegetation growing seasons for each individual pixel was counted for each year from 1982 to 2018. We implemented four phenology retrieval methods, including the amplitude threshold method, the second-order derivative method, the third-order derivative method, and the curvature change rate method, to retrieve four key phenological metrics for each vegetation growth cycle, including the start of the growing season (SOS), maturity, senescence, and the end of the growing season (EOS). The results show that the phenological metrics retrieved using different phenology retrieval methods have similar patterns of global spatial distribution. From 1982 to 2018, the timing of both maturity and senescence within a year advanced in the Northern Hemisphere and the timing of SOS delayed in the Southern Hemisphere. The phenological metrics extracted from in-situ data such as the USA National Phenology Network (USA-NPN), the Pan European Phenology Database (PEP725), and flux tower measurements were positively correlated with satellite-derived phenological metrics. Despite the effects of mismatching spatial scales, the retrieved phenological metrics based on 5 km AVHRR data were consistent with those based on 500 m Moderate-resolution Imaging Spectroradiometer (MODIS) data and 30 m fused satellite data at both site-scale and regional-scale. The developed dataset released for usages and applications on global land surface dynamics offers potential end users options for choosing desirable phenological metrics derived from different methods.

1. Introduction

Land surface phenology refers to the recurring cycle events of the land surface often triggered and driven by climate factors. Land surface phenology reflects the timing and duration of the growing season of terrestrial vegetation and its feedback to the climate system (Joiner et al., 2014). Land surface phenology controls ecosystem structures and functions and affects a wide range of land surface processes, such as ecosystem carbon sequestration and the energy balance between the land surface and the atmosphere (Seyednasrollah et al., 2019). An increasing number of studies assessed changes in vegetation phenology to quantify the impacts of climate changes on ecosystems (Chen et al., 2019; Liu et al., 2017). High-quality land surface phenology products have become increasingly important to understand the behavior of ecosystems under a changing climate.

Satellite observations that can capture the characteristics of land surface dynamics over a large geographic region have become popular for large-scale land surface phenology studies (Piao et al., 2019; White et al., 1997). For example, Piao et al. (2011) studied changes in vegetation phenology for over 25 years in temperate and boreal Eurasia based on Global Inventory Modeling and Mapping Studies (GIMMS) Normalized Difference Vegetation Index (NDVI) data. Høgda et al.

* Corresponding author.
E-mail address: xinqinchuan@mail.sysu.edu.cn (Q. Xin).

https://doi.org/10.1016/j.ecolind.2023.110262
Received 12 February 2023; Received in revised form 11 April 2023; Accepted 13 April 2023
Available online 22 April 2023

(2013) used GIMMS NDVI data to extract vegetation phenology metrics and found that vegetation growth patterns in the Nordic region showed prominent north–south differences. Zeng et al. (2013) compared trends in land surface phenology retrieved using Advanced Very High Resolution Radiometer (AVHRR), Moderate Resolution Imaging Spectroradiometer (MODIS), and Systeme Probatoire d'Observation de la Terre (SPOT) NDVI data, respectively, at high latitudes. Observational data acquired from various satellite sensors were used to retrieve land surface phenological metrics in a number of studies, delivering satellite-based land surface phenology dataset would be helpful to a wide range of applications (Hmimina et al., 2013; Soudani et al., 2008; Zhang et al., 2003).

Multiple methods have been developed to retrieve land surface phenology metrics from satellite-derived vegetation index time series. The main idea for most of these methods is to identify the turning points in the time series of satellite-derived vegetation index. For example, the thresholding methods apply thresholds for seasonal amplitudes (or absolute values) to time series of vegetation index to extract the timing of key phenological metrics (Fischer, 1994; Justice et al., 1985; White et al., 1997; Wu et al., 2017). The curve derivative methods identifies the timing of key phenological metrics based on the extreme values in the first or higher order derivatives of vegetation index time series (Sakamoto et al., 2005; Yu et al., 2003). The delayed moving average method extracts the timing of key phenological metrics by searching for the intersections of the vegetation index time series and their moving average curves (Reed et al., 1994). The function fitting methods fit the vegetation index time series with specific functions (e.g., Logistic and Gaussian functions) and identifies the timing of key phenological metrics based on the turning points of the fitted curves (Elmore et al., 2012; Fisher et al., 2006; Jönsson and Eklundh, 2004; Klosterman et al., 2014; Zhang et al., 2003). Despite that studies have applied the developed methods to retrieve land surface phenology metrics from regional to global scales (Piao et al., 2011; Xie et al., 2022; Yan et al., 2019; Zhang et al., 2003), different phenology retrieval methods could produce varied results and there is a need to enhance the interpretation of phenology retrieval methods.

Evaluation of satellite-retrieved phenological metrics based on ground-based observations is essential to the development and application of land surface phenology products (Donnelly et al., 2022). Traditional ground observations require observers visiting sites at regular time steps and provide phenological records for individual stands (Menzel et al., 2006; Schwartz et al., 2006). Ground-based phenology observation networks have become available in countries, including the Pan European Phenology Project (PEP725) (Templ et al., 2018), the Chinese Phenological Observation Network (CPON) (Dai et al., 2014; Ge et al., 2015; Guo et al., 2015), the USA National Phenology Network (USA-NPN) (Glynn and Owen, 2015), and the PhenoCam network (Hufkens et al., 2018; Seyednasrollah et al., 2019). A few studies found that satellite-derived phenology metrics have low correlations with ground-based phenological records due to mismatched spatial scales and varied definitions of phenology metrics (Ding et al., 2016; Zhang et al., 2003), and positive correlations between satellite-retrieved phenological metrics and ground-based observations were found in our previous studies (Wu et al., 2021; Xin et al., 2020). To understand the performance of satellite-based land surface phenology products, it is helpful to evaluate derived phenological metrics using ground-based observations while accounting for the effects of spatial scales.

Despite that existing satellite-based phenology studies favor time series data from moderate/coarse resolution sensors such as AVHRR and MODIS, there is a need to promote the development of global land surface phenology products due to limitations in sensor and data quality. MODIS has higher spatial resolution and better data quality than AVHRR, whereas AVHRR has nearly 20 years longer time series data than MODIS. For example, global land surface phenology product derived from the MODIS data (MCD12Q2) applied the thresholding method to retrieve the timing of phenology metrics dating back to 2001. The product offers results obtained from an empirical method and has found to have considerable missing values in the Southern Hemisphere. A global land surface phenology dataset developed based on AVHRR data (Wu et al., 2021) contains phenological metrics extracted from six phenology retrieving methods dating back to 1982, and it delivers the timing of two key phenological metrics within a calendar year, i.e., the start of the growing season (SOS) and the end of the growing season (EOS). The developed dataset had drawbacks as it did not account for multiple growing seasons of vegetation.

The main objectives of this study are to 1) develop a long-term global land surface phenology dataset based on the AVHRR data by applying multiple phenology retrieving algorithms, 2) improve phenology retrieving algorithms by accounting for multiple growing seasons and multiple seasonal phenological metrics in a year, and 3) assess satellite-retrieved phenological metrics using field data. We aim to improve the product previously developed (Wu et al., 2021; Xin et al., 2020) by applying different methods to retrieve the timing of phenological metrics, including SOS, maturity, senescence and EOS, for the time period from 1982 to 2018, and account for multiple growing seasons of vegetation. We attempt to assess the performance of different phenology retrieving algorithms by evaluating using ground-based observations and flux tower data, and analyze the scale effects when retrieving vegetation phenology from satellite data at both site and regional scales.

2. Data collection

2.1. Satellite data

Land Long Term Data Record (LTDR) developed by National Aeronautics and Space Administration (NASA) provides long-term data from multiple satellite platforms (https://landweb.modaps.eosdis.nasa.gov/cgi-bin/ltdr/ltdr/ltdrPage.cgi) (Pedelty et al., 2007). Version 5 LTDR daily land surface reflectance dataset (AVH09C1) was used to calculate time series of two-band enhanced vegetation index (EVI2) on a daily basis (Jiang et al., 2008). AVH09C1 derived from the AVHRR data implements processes such as orbital drift correction, sensor calibration, atmospheric correction, and bidirectional reflectance distribution function (BRDF) correction. It has a spatial resolution of 0.05° and dates back to July 1981. Note that some inconsistencies were observed at northern high latitudes (~60° N) in the AVHRR record, possibly due to calibration issues.

Because AVH09C1 has considerable amount of missing data in the years of both 1994 and 1997, we downloaded global GIMMS Leaf Area Index third generation (LAI3g) data (Zhu et al., 2013) from the releasing website (ftp://crsftp.bu.edu/cliveg/) for both years. GIMMS LAI3g was generated based on GIMMS NDVI and MODIS LAI data using a neural network algorithm. GIMMS LAI3g had been widely used for studies and applications on the monitoring and modeling of global vegetation. The dataset has a spatial resolution of 1/12°and a time step of 15 days. GIMMS LAI3g in 1994 and 1997 were used as substitution data to AVH09C1 for retrieving the timing of land surface phenology metrics.

We also used remote sensing data from both MODIS and Landsat, which have higher spatial resolution than AVHRR, for assessing the performance of the algorithm used to extract phenological metrics. The MODIS data were downloaded from the website of National Aeronautics and Space Administration (https://ladsweb.modaps.eosdis.nasa.gov/), and the Landsat data were downloaded from the website of United States Geological Survey (https://earthexplorer.usgs.gov/). We used MODIS products to make comparisons with the results extracted using algorithms in this study. The MODIS land cover type product (MCD12Q1) provides global land cover types at 500 m spatial resolution at annual time steps and contains six different classification schemes. We selected the University of Maryland (UMD) classification schemes in MCD12Q1 to extract vegetated areas (i.e., forests, shrublands, grasslands, and crops) on a global scale. MCD12Q2 delivers the timing of land surface phenology metrics on a global scale at 500 m spatial resolution. The

Table 1
Site information.

site name	latitude	longitude	years	elevation
SSA Old Aspen	53.63° N	106.20° W	2001–2006	601 m
Morgan Monroe State Forest	39.32° N	86.41° W	2001–2005	275 m
Univ. of Mich. Biological Station	45.56° N	84.71° W	2001–2007	234 m
Willow Creek	45.81° N	90.08° W	2001–2005	515 m

product contains the number of vegetation growing cycles per year and the dates of key phenological metrics for each vegetation growing cycle. We compared the phenological metrics extracted from AVHRR with those extracted from MCD12Q2 on a global scale. In addition, to further test and assess the phenology retrieval algorithms, we used both the MODIS land surface reflectance product (MOD09Q1) and the Landsat land surface reflectance data (Thematic Mapper (TM) and Operational Land Imager (OLI)) to fuse and generate time series of high-spatial-resolution satellite data (Chen et al., 2021). MOD09Q1 is an 8-day composite land surface reflectance product at a spatial resolution of 250 m. Landsat TM and OLI include 30 m multispectral images with 16-day revisiting time intervals. We chose two regions of Landsat scene (i.e., Path 13 / Row 30 and Path 25 / Row 28) as the test and assessment areas, corresponding to MODIS tiles h12v04 and h11v04. There are two main reasons for selecting these two regions. Firstly, the dominant land cover type in both regions is deciduous broadleaved forest with distinctive phenological characteristics. Secondly, two flux tower sites used in this study are located in these areas (i.e., Harvard Forest at Path 13/Row 30 and Willow Creek at Path 25/Row 28), enabling a comparison of phenological metrics extracted from different satellite sensors at both the site and regional scales.

2.2. Field observation data

To assess satellite-derived phenological metrics, we used ground-based phenology records and flux tower observations. The USA National Phenology Network (USA-NPN) collects ground-based phenology records that contain 243 phenological metrics for more than 400 plant types at nearly 3,000 sites. When processing the USA-NPN data, we treated the phenology records in deciduous vegetation from 2007 to 2017 that were described as "breaking leaf buds" as SOS, which included 5493 records from 1419 observation sites. We also treated the phenology records from 2008 to 2013 that were described as "all leaves fallen (deciduous)" as EOS, which included 297 records from 81 observation sites. Additionally, we treated the phenology records in deciduous vegetation from 2008 to 2013 that were described as ">=75% of full leaf size" as maturity, which included 481 records from 211 observation sites.

The Pan European Phenology Database (PEP725) contains nearly 12 million ground phenology records that include 46 phenological metrics coming from 121 plant species (Templ et al., 2018). Phenology metrics in PEP725 are defined according to the Biologische Bundesanstalt, Bundessortenamt and Chemical industry (BBCH) code (Meier, 1997). We chose the *Betula* observation records from 2002 to 2016 in PEP725 and processed the records described as "leaf unfolding with first visible leaf stalk" (BBCH code 11) as SOS, which included 24,517 records from 5073 observation sites. The records of *Betula* described as "autumnal coloring of leaves" (BBCH code 94) were treated as EOS, which included 22,742 records from 4001 observation sites. Additionally, we selected the *Vaccinium* observation records from 2000 to 2013 in PEP725 and treated the records described as "leaves beginning to discolor" (BBCH code 92) as senescence, which included 515 records from 91 observation sites.

Researchers in Harvard Forest have recorded phenology metrics of woody plants since spring in 1990 (O'Keefe, 2021). All observed tree individuals are located within 1.5 km of the Harvard Forest headquarters (42.535°N, 72.185°W) at the elevations between 335 and 365 m. We used the phenology observation records (1990–2018) acquired at Harvard Forest to evaluate satellite-derived phenological metrics.

Given the differences between ground-based and satellite-based definitions of phenology metrics, we also used LAI time series data from flux tower observations to assess the performance of satellite-derived phenology metrics. Richardson et al. (2012) conducted field experiments at four deciduous broadleaf forest sites (Table 1) to provide daily LAI measurements. We applied 20% of the seasonal amplitude to annual time series curve of LAI for extracting the timing of both SOS and EOS, and applied 70% of the seasonal amplitude to annual time series curve of LAI for extracting the timing of maturity and senescence during vegetation growing seasons.

2.3. Supplementary data

We attempt to account for multiple vegetation growth cycles in the produced product, and thus used the Global Cropping Intensity (GCI) dataset and its validation samples in the work of Liu et al. (2021) to assess the accuracy of the derived number of vegetation growth cycles in a calendar year. The GCI dataset spans from 2001 to 2019 with a spatial resolution of 250 m. The validation sample sites are all arable land types obtained by valid manual interpretation of EVI time series curves of Finer Resolution Observation and Monitoring of Global Land Cover (FROM-GLC) products. There are 2492 sample sites for each year from 2001 to 2019. Based on validation samples, GCI was assessed to have a mean overall accuracy of 89%.

3. Methods

We processed the AVHRR EVI2 time series as smoothed gap-filled time series of EVI2 data to reduce the impact of clouds and noise. We developed an algorithm to identify vegetation cycles from the smoothed EVI2 time series. We fitted the time series of EVI2 for each vegetation cycle using a logistic function and extracted four phenological metrics (i.e., SOS, maturity, senescence, and EOS) for each vegetation cycle using four phenology retrieval methods. Compared to our previously published study, the key improvements to our algorithms are to account for multiple growing seasons and include two more phenology metrics in the produced dataset. Details regarding to our algorithms to extract phenology metrics are explained as follows.

3.1. Processing time series of EVI2 data

Based on the quality assessment data for the AVH09C1 product, we replaced the data identified as snow with the closest snow-free data in the EVI2 time series and used the median of the 7-point moving window to replace outliers in the time series that differed from that median by more than three standard deviations. In addition, we used spline interpolation to fill up the missing data in the EVI2 time series and Savitzky-Golay (SG) filtering (Savitzky et al., 1964) to smooth the EVI2 time series.

3.2. Identifying vegetation growth cycles

We identified vegetation growth cycles for each calendar year from the processed time series of EVI2 data. Because growing cycles in the Southern Hemisphere are different from those in the Northern Hemisphere, we processed two consecutive years of EVI2 time series from six months preceding to six months following a calendar year and identified vegetation growth cycles for the corresponding calendar year.

A complete vegetation growth cycle consists of a vegetation green-up phase and a vegetation brown-down phase. The vegetation green-up (or brown-down) phase corresponds to a period of time when EVI2 increases (or decreases) in a monotonous manner. Specifically, the

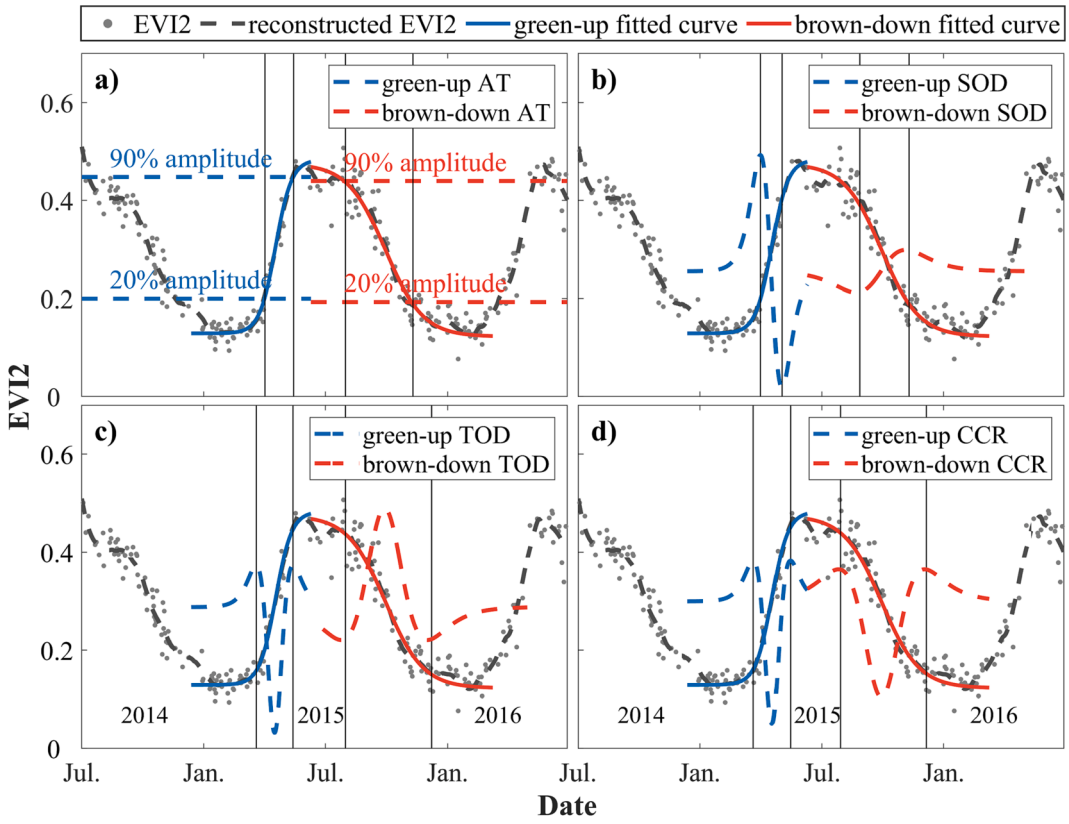

Fig. 1. Schematic diagrams of four phenology retrieval methods using AVHRR-EVI2 data, including a) AT, b) SOD, c) TOD, and d) CCR. The four vertical lines in the figure represent SOS, maturity, senescence and EOS from left to right.

vegetation green-up phase is identified as the sustained period of increase from local minimum to local maximum in EVI2 time series, while the vegetation brown-down phase is identified as the time period of sustained decrease from local maximum to local minimum in EVI2 time series. In order to eliminate slight increases (or decreases) in EVI2 unrelated to vegetation growth in the two-year EVI2 time series and to identify valid vegetation growth cycles, we used the following heuristics: (1) the duration of any identified period of sustained increase or decrease in EVI2 should be greater than 45 days and no more than 260 days; (2) the ratio of the local maximum EVI2 to the corresponding local minimum EVI2 should be not less than 1.5, or the difference between the local maximum EVI2 and the corresponding local minimum EVI2 should be at least 0.15; (3) if the start or end of the monotonic variation in EVI2 is in a year adjacent to the target calendar year, the duration of the sustained increase or decrease in EVI2 in the target calendar year shall be greater than 50% of its total duration of sustained increase or decrease. This process is repeated and the two-year EVI2 time series is partitioned into valid vegetation growth cycles.

The number of annual vegetation growing seasons can then be determined by simply counting the number of valid vegetation green-up and brown-down phases. Single growing season denotes areas with one and only one valid green-up phase and brown-down phase in the EVI2 time series, double growing season denotes areas with two and only two valid green-up or brown-down phases in the EVI2 time series, and triple growing season denotes areas with three and only three valid green-up or brown-down phases in the EVI2 time series. Note that although we identified pixels with triple growing seasons, we extracted the phenological metrics for up two vegetation growing seasons per year. In other words, if there are three growing seasons, the number of annual vegetation growing seasons metric will reflect the correct number, but phenological metrics will not be retrieved for the third growing season. Furthermore, we identified vegetated areas that did not exhibit significant seasonal changes and had EVI2 values greater than 0.35 for more than 45 days of the year as single growing season. In summary, the number of annual vegetation growing seasons metric contains four values of 0, 1, 2, and 3, indicating no growing season, single growing season, double growing season, and triple growing season, respectively.

3.3. Fitting time series of EVI2 data

To flexibly simulate vegetation growth under various conditions, we used logistic curve fitting functions (Zhang et al., 2003) to fit the EVI2 time series during the green-up phase (Eq. (1)) and the brown-down phase (Eq. (2)) for each vegetation growth cycle:

$$EVI2_{green-up}(t) = \frac{c}{1+e^{a+b*t}} + m \quad (1)$$

$$EVI2_{brown-down}(t) = -\frac{c}{1+e^{a+b*t}} + n \quad (2)$$

where t represents the time in days, both a and b are fitting parameters, c is the difference between maximum and minimum EVI2 in a vegetation growth cycle, m is minimum EVI2 in the vegetation growth cycle, and n is maximum EVI2 in the vegetation growth cycle.

3.4. Extracting phenological metrics

Extraction of phenological metrics is performed on each identified vegetation growth cycle. We applied four methods (Fig. 1), including the amplitude threshold (AT) method (Fischer, 1994; Jönsson and Eklundh, 2004), the second-order derivative (SOD) method (Sakamoto et al., 2005), the third-order derivative (TOD) method (Tan et al., 2011) and the curvature change rate (CCR) method (Zhang et al., 2003), to identify key turning points in the fitted EVI2 time series and derive the timing of key phenological metrics.

Table 2
Evaluation of phenological metrics using phenology observation networks.

Phenological metrics	Methods	PEP725		USA-NPN	
		r	RMSE (days)	r	RMSE (days)
SOS	AT	0.43**	37.27	0.58**	29.36
	SOD	0.62**	41.27	0.57**	30.71
	TOD	0.74**	54.57	0.51**	40.51
	CCR	0.73**	54.42	0.52**	39.55
maturity	AT	/	/	0.62**	17.16
	SOD	/	/	0.74**	14.03
	TOD	/	/	0.62**	17.66
	CCR	/	/	0.62**	17.64
senescence	AT	0.44*	31.97	/	/
	SOD	0.68*	24.06	/	/
	TOD	0.49	32.32	/	/
	CCR	0.46	32.77	/	/
EOS	AT	0.43	25.32	0.59**	26.70
	SOD	0.61	28.78	0.58**	28.75
	TOD	0.66	39.18	0.01	55.70
	CCR	0.64	38.25	0.10	52.80

* denotes $p < 0.05$, ** denotes $p < 0.01$.

Table 3
Evaluation of phenological metrics using flux tower field data.

Phenological metrics	Methods	Harvard Forest		relative LAI	
		r	RMSE (days)	r	RMSE (days)
SOS	AT	0.68**	6.69	0.76**	26.83
	SOD	0.68**	6.56	0.69**	28.42
	TOD	0.63**	8.80	0.50**	49.43
	CCR	0.63**	8.89	0.50**	48.05
maturity	AT	0.54*	4.05	0.71**	15.25
	SOD	0.83**	2.61	0.85**	8.32
	TOD	0.50*	4.15	0.69**	17.21
	CCR	0.51*	4.23	0.69**	17.39
senescence	AT	0.50*	9.86	0.61**	15.97
	SOD	0.64**	6.17	0.68**	12.42
	TOD	0.49*	10.30	0.60**	16.51
	CCR	0.49*	10.34	0.59**	16.55
EOS	AT	0.41*	8.84	0.81**	10.52
	SOD	0.42*	8.64	0.81**	11.87
	TOD	0.36	13.03	0.69**	31.66
	CCR	0.35	13.23	0.83**	30.17

* denotes $p < 0.05$, ** denotes $p < 0.01$.

AT identifies the timing of key phenological metrics by applying thresholds to the amplitude of the EVI2 time series (Fig. 1a). We used a 20% amplitude threshold (Zhou et al., 2016) to extract the timing of SOS (or EOS), and a 90% amplitude threshold (Gray et al., 2019) to extract the timing of maturity (or senescence) in the vegetation growing season. SOD identifies the timing of phenological metrics according to local extreme points in the second-order derivative curve of the fitted EVI2 time series (Fig. 1b). When applying the method of SOD, SOS is identified as the date when the first local maximum occurs in the second-order derivative curve of vegetation green-up phase; maturity is identified as the date of when the first local minimum occurs in the second-order derivative curve of vegetation green-up phase; senescence is identified as the date when the first local minimum occurs in the second-order derivative curve of vegetation brown-down phase; and EOS is identified as the date when the first local maximum occurs in the second-order derivative curve of vegetation brown-down phase. TOD retrieves the timing of phenological metrics based on local extreme points in the third-order derivative curve of the fitted EVI2 time series (Fig. 1c). When applying the method of TOD, SOS (or maturity) is identified as the date when the first (or the second) local maximum occurs in the third-order derivative curve of vegetation green-up phase, whereas EOS (or senescence) is identified as the date when the first (or the second) local minimum occurs in the third-order derivative curve of vegetation brown-down phase. CCR identifies the timing of phenological metrics based on the local maximum in the curvature changes of EVI2 curves (Fig. 1d). When applying the method of CCR, SOS (or maturity) is identified as the date when the first (or the second) local maximum occurs in the curvature change curve of vegetation green-up phase. EOS (or senescence) is identified as the date when the first (or the second) local maximum in the curvature change curve of vegetation brown-down phase.

3.5. Assessing the derived phenological metrics

We used in-situ and remote sensing data to assess the derived phenological metrics. The Pearson's correlation coefficient (r) and Root Mean Square Error (RMSE) are used to quantify the performance of the phenology retrievals. Specifically, we first evaluated satellite-derived phenological metrics (i.e., SOS, maturity, senescence, and EOS) using ground-based phenology observations (i.e., USA-NPN and PEP725). Due to the different definitions of phenological metrics in the different datasets, maturity was assessed using USA-NPN data only and senescence was assessed using PEP725 data only. Then we evaluated SOS, maturity, senescence, and EOS using flux tower observations (i.e., Harvard Forest and relative LAI time series data). Next, we compared the phenological metrics extracted in this study with the MODIS phenological metrics. Note that our previous study has found that SOS (or EOS) extracted based on AVHRR data was consistent with SOS (or EOS) extracted based on MODIS data in terms of global distribution (Wu et al., 2021), therefore, this paper only focuses on the performance of two phenological metrics, maturity and senescence. Finally, we compared the phenological metrics extracted from different satellite data at the site scale and regional scale.

4. Results

4.1. Assessment

Ground-based phenology network observations, flux tower data and the MODIS global land surface phenology dataset were used to assess the performance of the phenology metrics extracted in this study. The details are as follows.

Firstly, the performances of the satellite-retrieved phenological metrics (i.e., SOS, maturity, senescence and EOS) were assessed using PEP725 and USA-NPN data (Table 2). When assessed using PEP725 data, SOS derived using all four phenology retrieval methods were significantly correlated with ground-based SOS. Senescence metrics derived using AT ($p < 0.05$) and SOD ($p < 0.05$) were significantly correlated with ground-based senescence metrics. None of the EOS derived using four phenology retrieval methods correlated significantly with ground-based EOS. When assessed using USA-NPN data, SOS and maturity metrics derived using AT, SOD, TOD, and CCR were significantly correlated with ground-based SOS and maturity metrics. EOS derived using AT ($p < 0.01$) and SOD ($p < 0.01$) were significantly correlated with ground-based EOS.

Secondly, observations from flux towers (i.e., Harvard Forest and relative LAI time series data) were used to assess the performances of satellite-retrieved SOS, maturity, senescence and EOS (Table 3). When assessed using Harvard Forest data, SOS, maturity, and senescence metrics derived using four phenology retrieval methods were significantly correlated with field SOS, maturity, and senescence metrics.

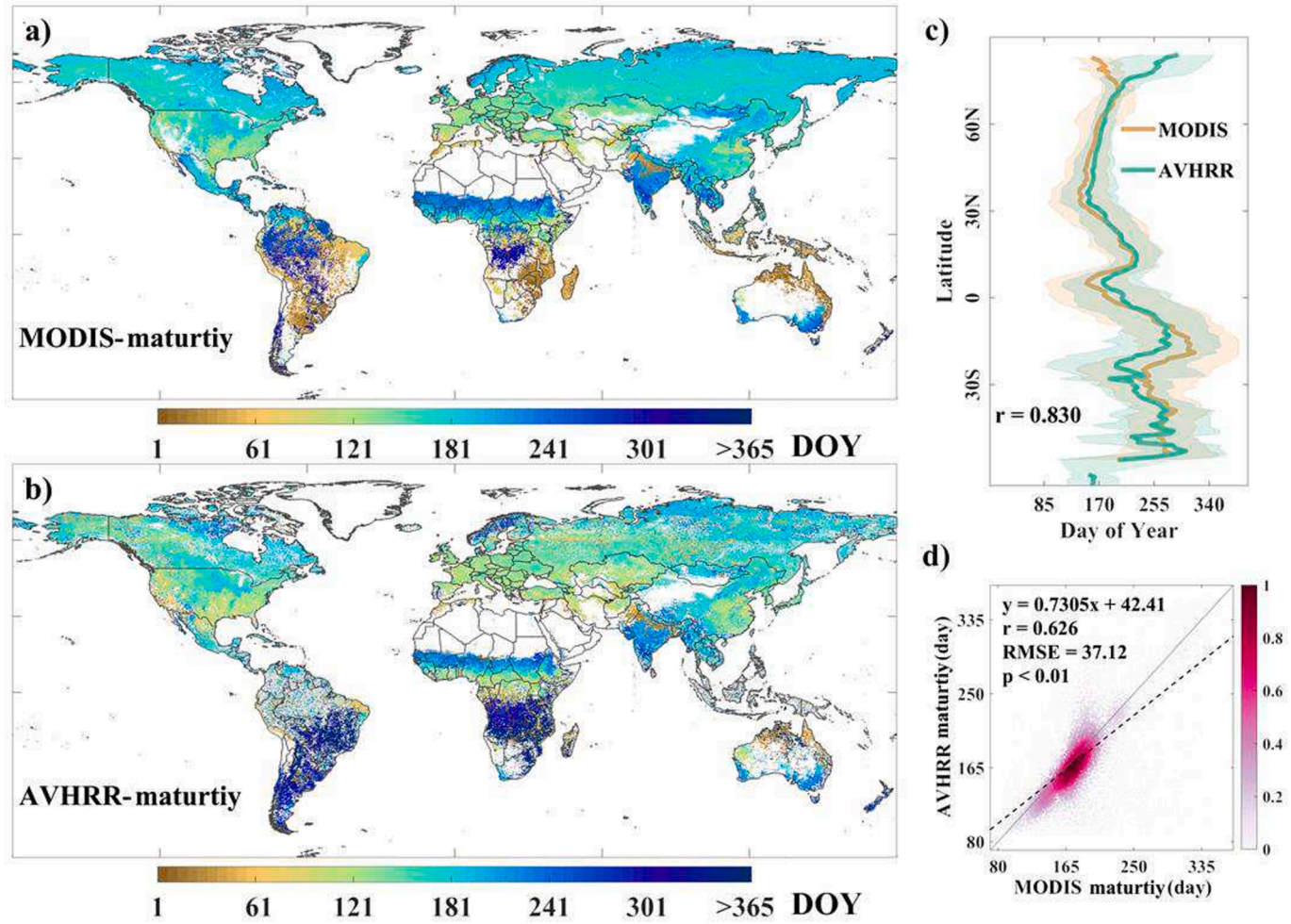

Fig. 2. Comparison of global AVHRR-maturity and MODIS-maturity in 2015.

Among them, SOD achieved the best performance with $r_{SOS} = 0.68$ and $RMSE_{SOS} = 6.56$ days; $r_{maturity} = 0.83$ and $RMSE_{maturity} = 2.61$ days; and $r_{senescence} = 0.64$ and $RMSE_{senescence} = 6.17$ days. EOS derived using AT ($p < 0.05$) and SOD ($p < 0.05$) were significantly correlated with ground-based EOS. When assessed using relative LAI time series data, SOS, maturity, senescence, and EOS derived using all four phenology retrieval methods were significantly correlated with field SOS, maturity, senescence, and EOS. Specifically, AT performed best in the extraction results of SOS ($r = 0.76$ and RMSE = 26.83 days); SOD showed the best performance in both maturity ($r = 0.85$ and RMSE = 8.32 days) and senescence ($r = 0.68$ and RMSE = 12.42 days) extraction results; EOS extracted using CCR exhibited the highest $r = 0.83$ and EOS extracted using AT exhibited the smallest RMSE = 10.52 days.

Finally, we used the phenological metrics from the MODIS land surface phenology dataset (MCD12Q2) to assess the phenological metrics extracted in this study. Fig. 2 compares the maturity retrieved from the AVHRR data (hereafter written as AVHRR-maturity) with maturity from the MCD12Q2 product (hereafter written as MODIS-maturity) in 2015. The spatial distribution of MODIS-maturity (Fig. 2a) and AVHRR-maturity (Fig. 2b) is generally consistent at the global scale, while they show obvious differences in the Eastern and Southeastern South America and Southeastern Africa. The timing of AVHRR-maturity for these regions is distributed in the second half of the year, while the timing of MODIS-maturity is mostly distributed in the first half of the year. Fig. 2c shows that the AVHRR-maturity is highly consistent with the MODIS-maturity in the latitudinal direction with a correlation coefficient r of 0.830. Fig. 2d shows the density scatter plot of AVHRR-maturity compared with MODIS-maturity, which exhibits a significant correlation with the r of 0.626 and the RMSE of 37.12 days.

Fig. 3 compares the senescence retrieved from AVHRR data (hereafter written as AVHRR-senescence) with senescence from the MCD12Q2 product (hereafter written as MODIS-senescence) in 2015. Overall, the spatial distribution of MODIS-senescence (Fig. 3a) and AVHRR-senescence (Fig. 3b) remain consistent at the global scale, while AVHRR-senescence is apparently earlier than MODIS-senescence in Indochina Peninsula of Southeast Asia and slightly later than MODIS-senescence in Eastern South America and Southern Africa. In the latitudinal direction, the variation of AVHRR-senescence remains consistent with MODIS-senescence with a correlation coefficient r of 0.826 (Fig. 3c). Fig. 3d shows that AVHRR-senescence is significantly correlated with MODIS-senescence with $r = 0.584$ and RMSE = 49.65 days. In addition, compared with MCD12Q2, the algorithm in this study did not detect seasonal changes in vegetation growth in tropical rainforest regions such as the Amazon Plain in South America and the Malay Archipelago in Southeast Asia.

4.2. Spatial distributions

We mapped the average distribution of the four phenological metrics (i.e., SOS, maturity, senescence and EOS) in the first growing season of each year extracted using SOD worldwide from 1982 to 2018 (Fig. 4a, 4b, 4c, and 4d). The dates of mean SOS and maturity gradually advanced from Arctic to the equator in the Northern Hemisphere. But the dates of mean SOS and maturity in parts of South and Southeast Asia are much

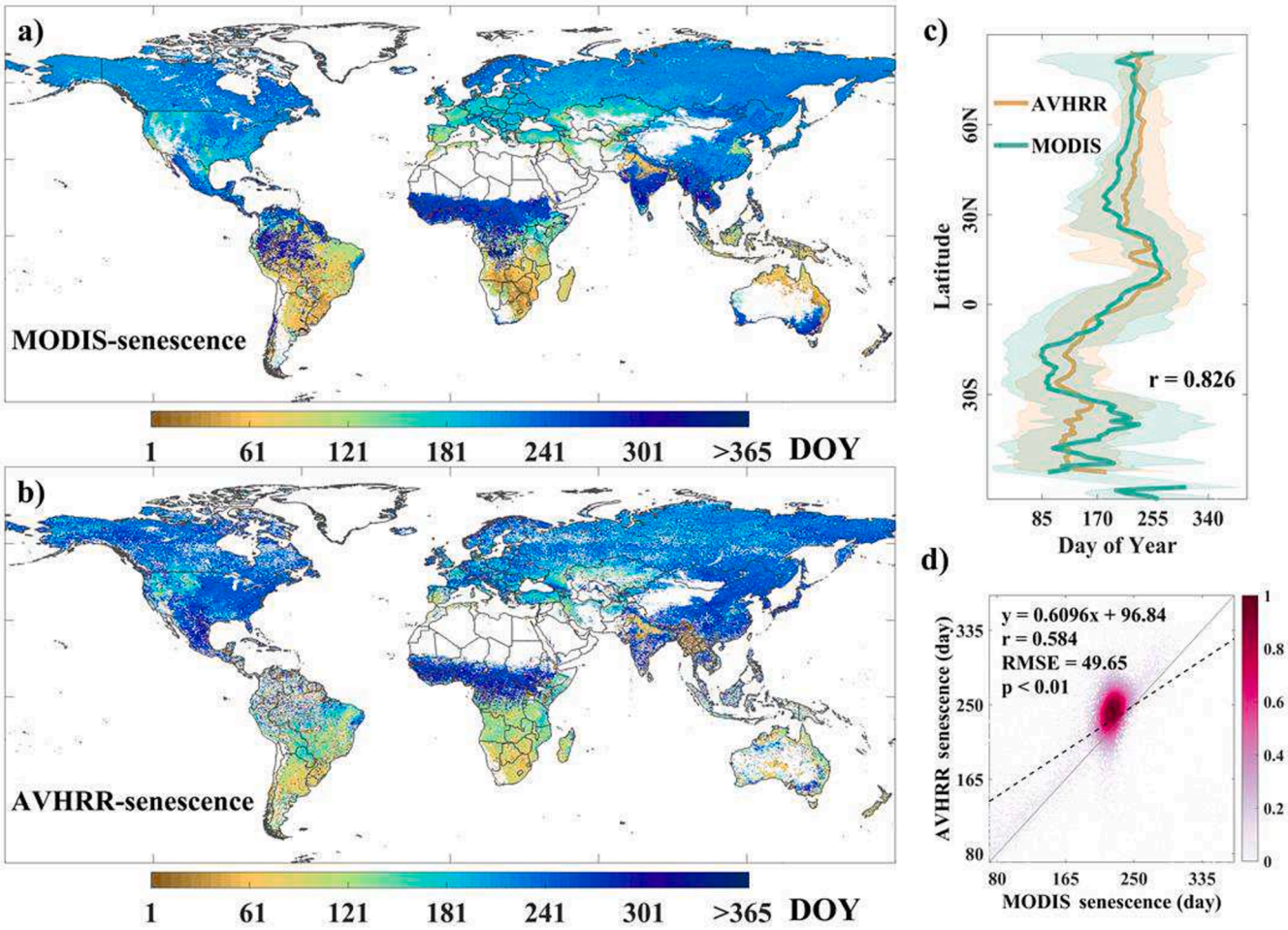

Fig. 3. Comparison of global AVHRR-senescence and MODIS-senescence in 2015.

later than in the neighboring regions. The trends of mean senescence and EOS are reversed, they are gradually delayed from north to south in most regions of the Northern Hemisphere. But the dates of mean senescence and EOS in parts of South and Southeast Asia are much earlier compared to neighboring regions. In the Southern Hemisphere, the dates of mean SOS and maturity are delayed with increasing latitude, but are earlier in the southern part of South America than in the surrounding regions. The dates of mean senescence and EOS are advanced with increasing latitude.

We also mapped the global distribution of SOS, maturity, senescence and EOS in the second vegetation growing season retrieved using SOD in 2015 (Fig. 4e, 4f, 4g, and 4h). The areas where the second vegetation green-up phase in a year was observed mainly include Northern China, Northern India, Central and Eastern Africa, Central United States, Southeastern South America, and Western Europe (Fig. 4e and 4f). As shown in Fig. 4g and 4h, the areas where the second vegetation brown-down phase in a year was observed mainly include Northern China, Northern India, Central and Eastern Africa, Central and Southeastern South America, Southeastern Asia and Western Europe.

Additionally, we mapped the global distribution of the number of vegetation growing seasons (taking 2015 as an example, Fig. 4i). Single growing season is found in most regions of the world. Double growing season is mainly found in the North China Plain, Northern India, Central Africa, Central and Southeastern South America, Southern Russia, Western Europe, and parts of North America. Triple growing seasons is observed mainly in Northern India, the North China Plain and parts of South America.

4.3. Temporal trends

We mapped the temporal trends of annual mean SOS, maturity, senescence and EOS retrieved using the four phenology retrieval methods in the Northern and Southern Hemispheres from 1982 to 2018. Note that we only explored temporal trends in phenological metrics for the first growing season of each year. In the Northern Hemisphere, the dates of annual mean SOS extracted using AT, SOD, TOD and CCR did not show significant trends over the past 37 years (Fig. 5a). The SOS extracted using TOD and CCR were close and significantly earlier than those extracted using AT and SOD. From 1982 to 2018, the dates of annual mean maturity extracted using AT and TOD were significantly advanced at 0.07846 day/year ($p < 0.05$) and 0.07998 day/year ($p < 0.05$), respectively (Fig. 5b). The dates of annual mean senescence extracted using AT, TOD and CCR exhibited significantly advanced trends of 0.1386 days/year ($p < 0.05$), 0.1793 days/year ($p < 0.01$) and 0.1801 days/year ($p < 0.01$), respectively, during the period 1986 to 2018 (Fig. 5c). Note that the date of maturity extracted using SOD was earlier than other methods, while the date of senescence extracted using SOD was later than other methods. The dates of annual mean EOS extracted using AT, SOD, TOD and CCR changed insignificantly during 1982–2018 (Fig. 5d). The EOS extracted using TOD and CCR were highly similar and significantly later than those extracted using AT and SOD.

In the Southern Hemisphere, from 1982 to 2018, the dates of annual mean SOS extracted using AT, SOD, TOD and CCR showed significantly delayed trends of 0.1957 days/year ($p < 0.05$), 0.2102 days/year ($p < 0.01$), 0.2750 days/year ($p < 0.01$) and 0.2686 days/year ($p < 0.01$), respectively (Fig. 5e). The SOS extracted using TOD and CCR were very

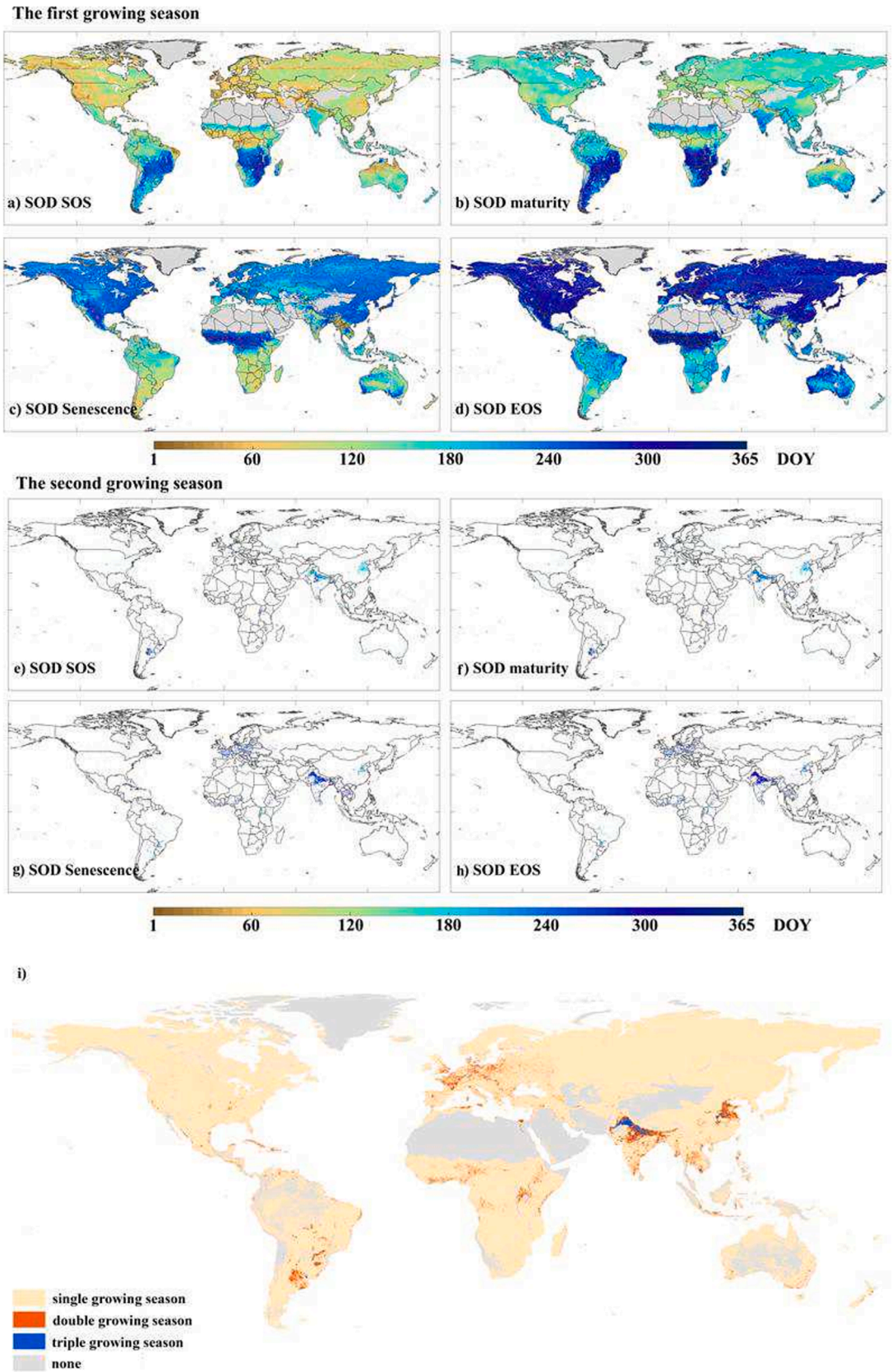

Fig. 4. Global spatial distribution of phenological metrics in the first growing season (a-d), phenological metrics in the second growing season (e-h) and the number of vegetation growing seasons (i).

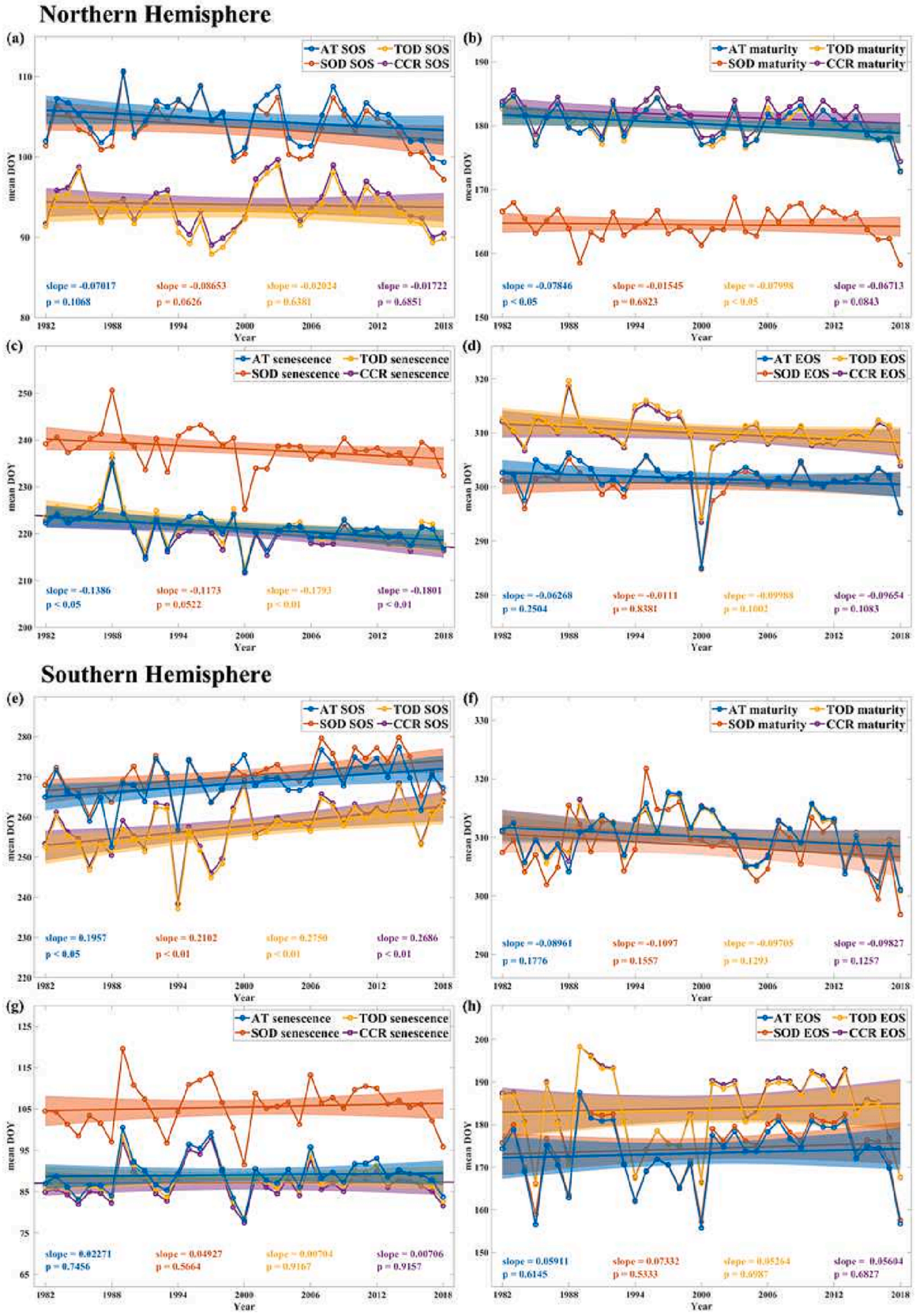

Fig. 5. Temporal trends (1982–2018) in SOS (a and e), maturity (b and f), senescence (c and g) and EOS (d and h) extracted using four methods (i.e., AT, SOD, TOD and CCR) in the Northern and Southern Hemispheres. The colored solid lines indicate the fitted trend lines and the colored bars indicate the 95% confidence intervals.

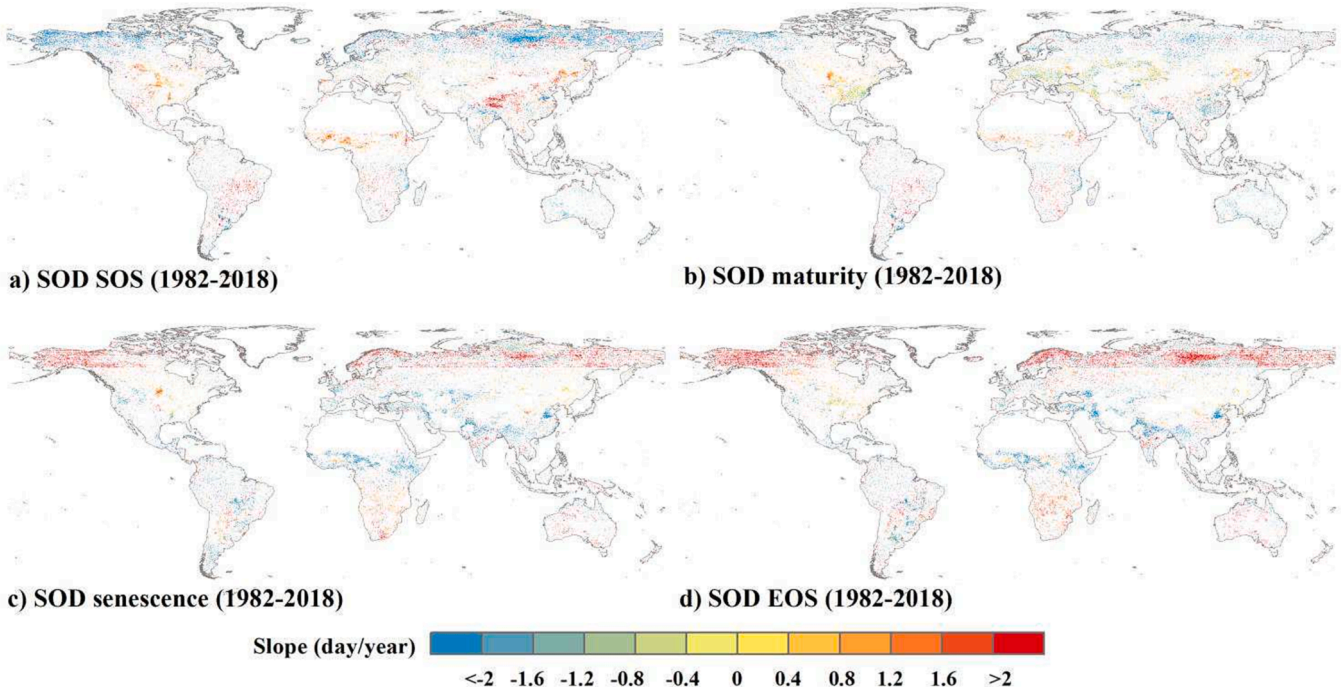

Fig. 6. Trends in the phenological metrics retrieved from the AVHRR data using SOD from 1982 to 2018, where a) is SOS, b) is maturity, c) is senescence, and d) is EOS.

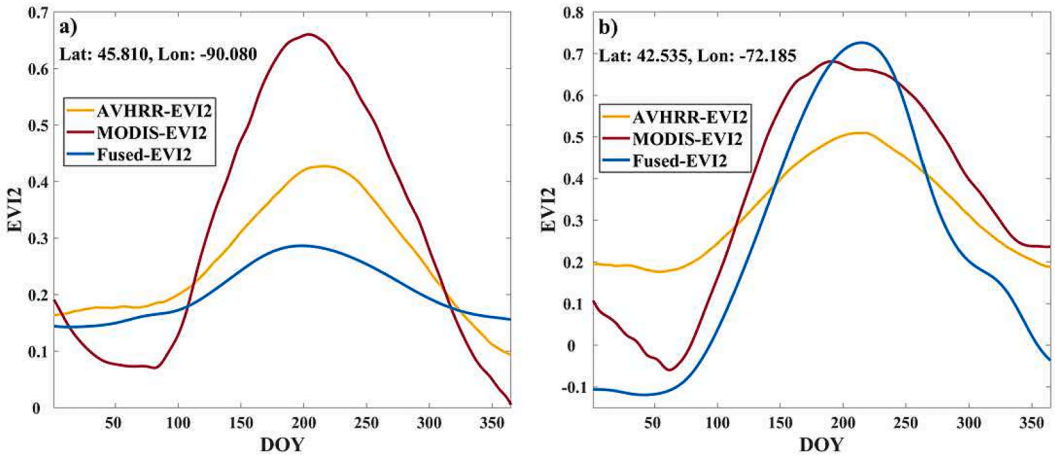

Fig. 7. Site-scale EVI2 time series at different spatial resolutions. a) is Willow Creek flux tower site in 2003, and b) is Harvard Forest flux tower site in 2015.

Table 4
Comparison of site scale phenological metrics based on EVI2 time series with different spatial resolutions and field data from flux towers.

Data source	Willow Creek (Lat: 45.810, Long: −90.080)				Harvard Forest (Lat: 42.535, Long: −72.185)			
	SOS (DOY)	maturity (DOY)	senescence (DOY)	EOS (DOY)	SOS (DOY)	maturity (DOY)	senescence (DOY)	EOS (DOY)
AVHRR data	114	175	266	332	101	162	259	324
MODIS data	120	158	259	340	92	141	264	320
Fused data	101	161	250	318	104	166	248	321
Flux tower data	141	155	269	292	128	149	285	293

close and earlier than those extracted using AT and SOD. The dates of annual mean maturity extracted using AT, SOD, TOD and CCR showed insignificantly advanced trends from 1982 to 2018 (Fig. 5f). The dates of annual mean senescence extracted using AT, SOD, TOD and CCR exhibited insignificant changes during the period 1986 to 2018 (Fig. 5g). The date of senescence extracted using SOD was later than those using other methods. Over the past 37 years, no significant trends were observed in the dates of mean EOS extracted using AT, SOD, TOD and CCR (Fig. 5h).

The trends of phenological metrics at each pixel were calculated at the 95% confidence level for the results retrieved by SOD (Fig. 6). Between 1982 and 2018, approximately 11.97% of the total pixels

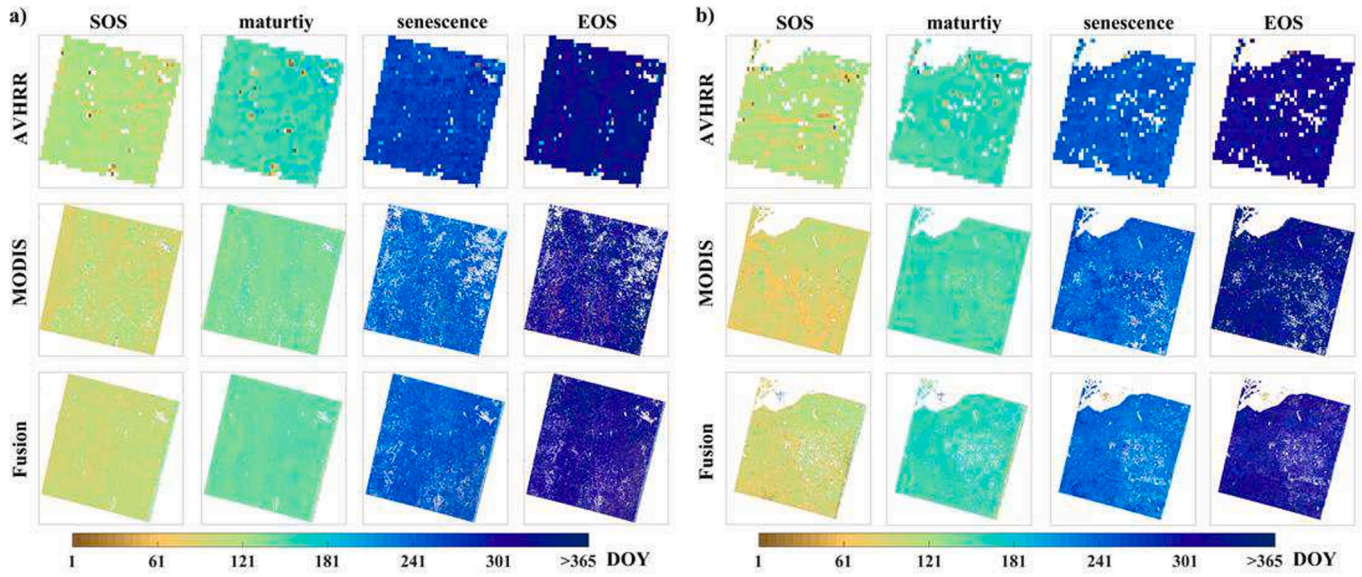

Fig. 8. Comparison of regional-scale phenology information at different spatial resolutions (taking the SOD retrieval results in 2015 as an example). a) represents the region of Landsat scene: Path 13 / Row 30 and b) represents the region of Landsat scene: Path 25 / Row 28).

Table 5
Comparison of regional-scale mean SOS, maturity, senescence and EOS retrieved from EVI2 time series data at different spatial resolutions.

Data source	Region 1 (Landsat scene: Path 13 / Row 30)				Region 2 (Landsat scene: Path 25 / Row 28)			
	Mean SOS (DOY)	Mean maturity (DOY)	Mean senescence (DOY)	Mean EOS (DOY)	Mean SOS (DOY)	Mean maturity (DOY)	Mean senescence (DOY)	Mean EOS (DOY)
AVHRR data	115	150	264	322	114	154	248	304
MODIS data	101	140	242	311	90	152	244	329
Fused data	102	145	244	305	97	157	236	301

exhibited significant changes in SOS, of which 7.29% showed an advancement. The proportion of significantly changed pixels in maturity accounted for 10.37% of the total pixels from 1982 to 2018, of which 7.42% exhibited advanced trends. Additionally, from 1982 to 2018, 10.58% of the total pixels exhibited significant changes in senescence, of which 5.48% showed significantly advanced trends and 5.10% had significantly delayed trends. Over the period of 1982 to 2018, the proportion of pixels with significant trends in EOS was 12.34% of the total pixels, while pixels with delayed trends accounted for 7.40%.

4.4. Spatial scale effects

Although satellite data has been widely used to retrieve phenological metrics, there are non-negligible scale effects between the phenological metrics extracted based on the remote sensing data from different sensors. Fig. 7 shows the site-scale EVI2 time series calculated based on the 5 km AVHRR, 500 m MODIS and 30 m Landsat-MODIS fusion data, respectively. At the site scale, both the specific values and the curve trajectories of the EVI2 time series extracted based on different sensors show significant differences. For example, the difference between MODIS-EVI2 and Fused-EVI2 peaks is 0.4 at the Willow Creek site. Comparison of the EVI2 time series between the two sites shows that the EVI2 time series extracted based on different sensors have no regular features in terms of the relative magnitude of the values and the trajectory changes of the curves.

Table 4 presents a comparison of site-scale SOS, maturity, senescence, and EOS based on different satellite sensors as well as flux tower data. At Willow Creek site, the maximum difference between the phenological metrics extracted based on different satellite data was 22 days and the minimum difference was 3 days. The timing of SOS and senescence derived from flux tower data were later than those derived from satellites, while the timing of maturity and EOS derived from flux tower data were earlier than the timing of satellite-derived maturity and EOS. At Harvard Forest site, the maximum difference between the phenological metrics extracted based on satellite data of different resolutions was 25 days and the minimum difference was 1 day. The phenological metrics derived from the flux tower data showed similar characteristics to the Willow Creek site except that the timing of maturity derived from MODIS data was earlier than the timing of maturity derived from the flux tower data.

Fig. 8 compares the regional-scale phenological metrics retrieved based on EVI2 time series data with different spatial resolutions. Although more spatial details are available in the high-resolution phenological metrics results for both regions, the 30 m, 500 m and 5 km resolution phenological metrics results are highly consistent in terms of regional spatial distribution.

Table 5 presents a comparison of the mean SOS, maturity, senescence and EOS at different spatial resolutions retrieved using the SOD method at the regional-scale. In Region 1, the dates of mean SOS, maturity and senescence derived from 500 m MODIS data were the earliest and those derived from 5 km AVHRR data were the latest, with the maximum differences of 14 days, 10 days and 22 days, respectively. The dates of mean SOS and senescence retrieved based on 500 m MODIS data were very close to those retrieved based on 30 m fused data, where the difference in mean SOS was 1 day and the difference in mean senescence was 2 days. The earliest and latest mean EOS were extracted from the 30 m fused data and 5 km AVHRR data, respectively, with a 17-day difference. In Region 2, the date of mean SOS retrieved based on MODIS data was the earliest and the date of mean SOS retrieved based on AVHRR data was the latest, with a difference of 24 days. The earliest mean maturity was derived from MODIS data, and the latest mean maturity was derived from fused data, with a difference of 5 days. The

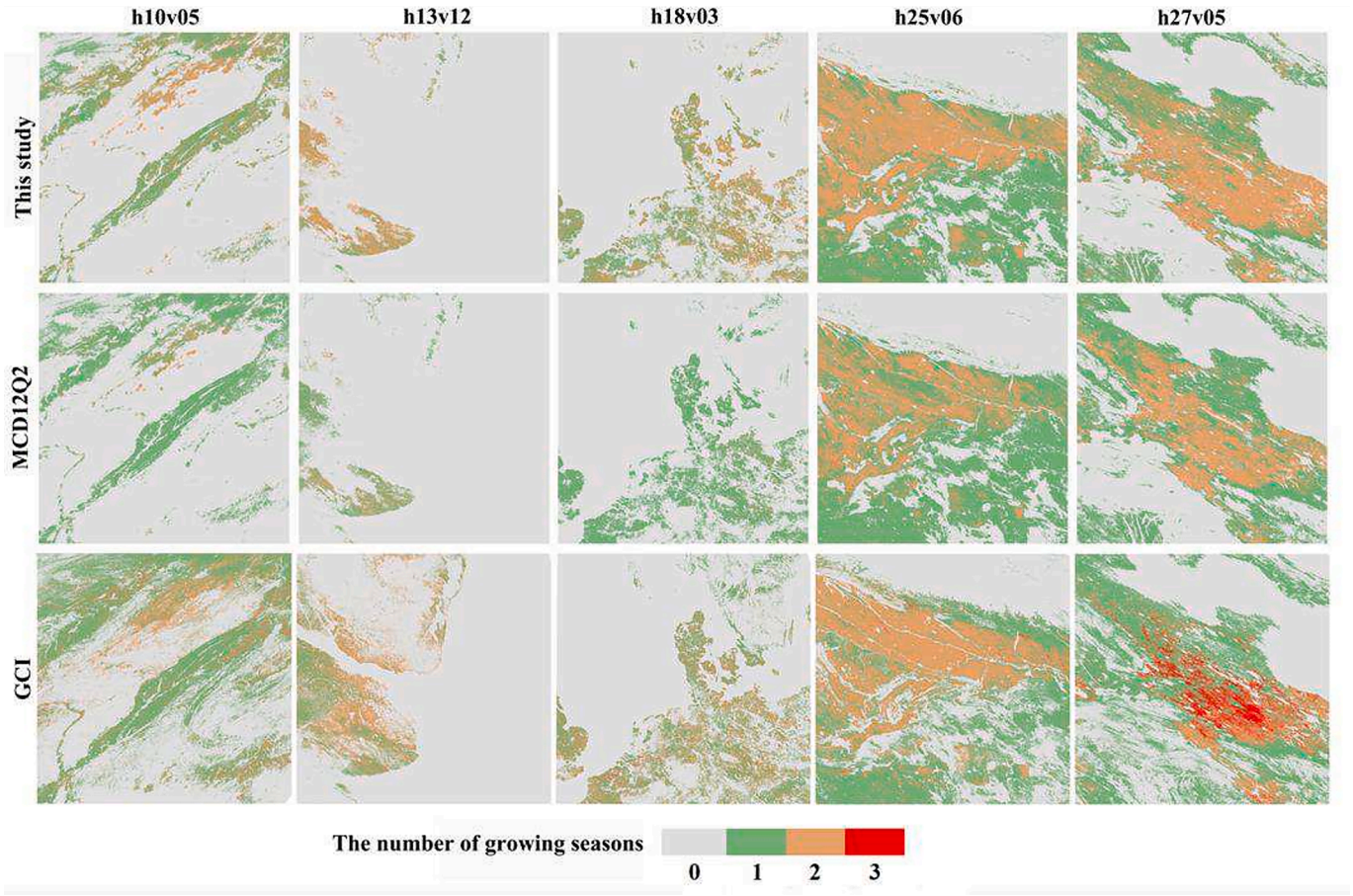

Fig. 9. Comparison of the number of vegetation growing seasons extracted by the three algorithms across the five MODIS tiles (i.e., h10v05, h13v12, h18v03, h25v06, and h27v05) in 2012.

difference between the earliest mean senescence derived based on the fused data and the latest derived based on the AVHRR data was 12 days. The earliest mean EOS retrieved from the fused data and the latest retrieved from the MODIS data are 28 days apart.

5. Discussion

Here, we develop a global land surface phenology dataset from 1982 to 2018 based on AVHRR data using four phenology retrieving methods. The extracted dataset provides records of phenological information for up to two vegetation growing seasons, such as multi-cropping, precipitation-driven green-up events, and other phenological regimes that deviate from the common single annual green-up or brown-down event pattern, with specific phenological metrics including SOS, maturity, senescence, and EOS. The phenological metrics extracted by different methods remain largely consistent in terms of spatial distribution (Figs. 4, A1, and A2). Notably, we found that the quality of the LTDR land surface reflectance product (AVH09C1) was severely declined above 60° N. Due to some inconsistencies in AVH09C1 product at high latitudes (~60° N), the phenological metrics retrieved accordingly are also discontinuous in this region. For example, SOS exhibits significant discontinuities above 60° N due to declined data quality. Hence, AVHRR data should be used with caution above 60° N.

As phenological metrics extracted using different methods vary greatly (Gan et al., 2020; Wu et al., 2021; Xin et al., 2020), it is necessary to evaluate the performances of different phenology retrieving methods using multiple field data. As shown in Tables 2 and 3, the four phenology retrieving methods used in this study, AT, SOD, TOD and CCR, have been proven to be effective in extracting SOS, maturity, senescence, and EOS by ground-based observations. Nevertheless, due to differences in spatial scales and definitions of phenological metrics, satellite-derived phenology products may not be fully consistent with those based on ground-based observations. The satellite-derived phenological metrics have different characteristics from those of ground-based observations, and reflect mainly the phenological changes of overall mixed type. The ground-based observations tend to select vegetation that is more sensitive to climate, and therefore, the satellite-derived phenological metrics are generally later than the ground-based phenological metrics. For the phenology dataset generated in this study, users can flexibly choose the phenological metrics derived by different methods according to the actual situation. For example, if the users need to acquire phenological metrics that are the closest with ground-based observations, it is recommended using the SOS and EOS extracted by AT and maturity and senescence extracted by SOD.

In addition to the site-scale assessment, we also compared the dataset extracted in this study and MCD12Q2 at the global scale. Fig. 2 shows that the spatial distribution of MODIS-maturity and AVHRR-maturity remains largely consistent at the global scale, but there are significant differences in eastern and southeastern South America and southeastern Africa. In these regions, the timing of maturity extracted in this study is concentrated in the second half of the year, while the timing of maturity extracted in MCD12Q2 is concentrated in the beginning of the year. As we know, the vegetation growing season in the Southern Hemisphere is reversed to that of the Northern Hemisphere. Therefore, one possible reason is that the MCD12Q2 product extracted the phenological metrics from the previous year's vegetation growth cycle. Similarly, the senescence extracted in this study and MCD12Q2 are consistent in their global spatial distribution. However, in Indochina Peninsula of Southeast Asia,

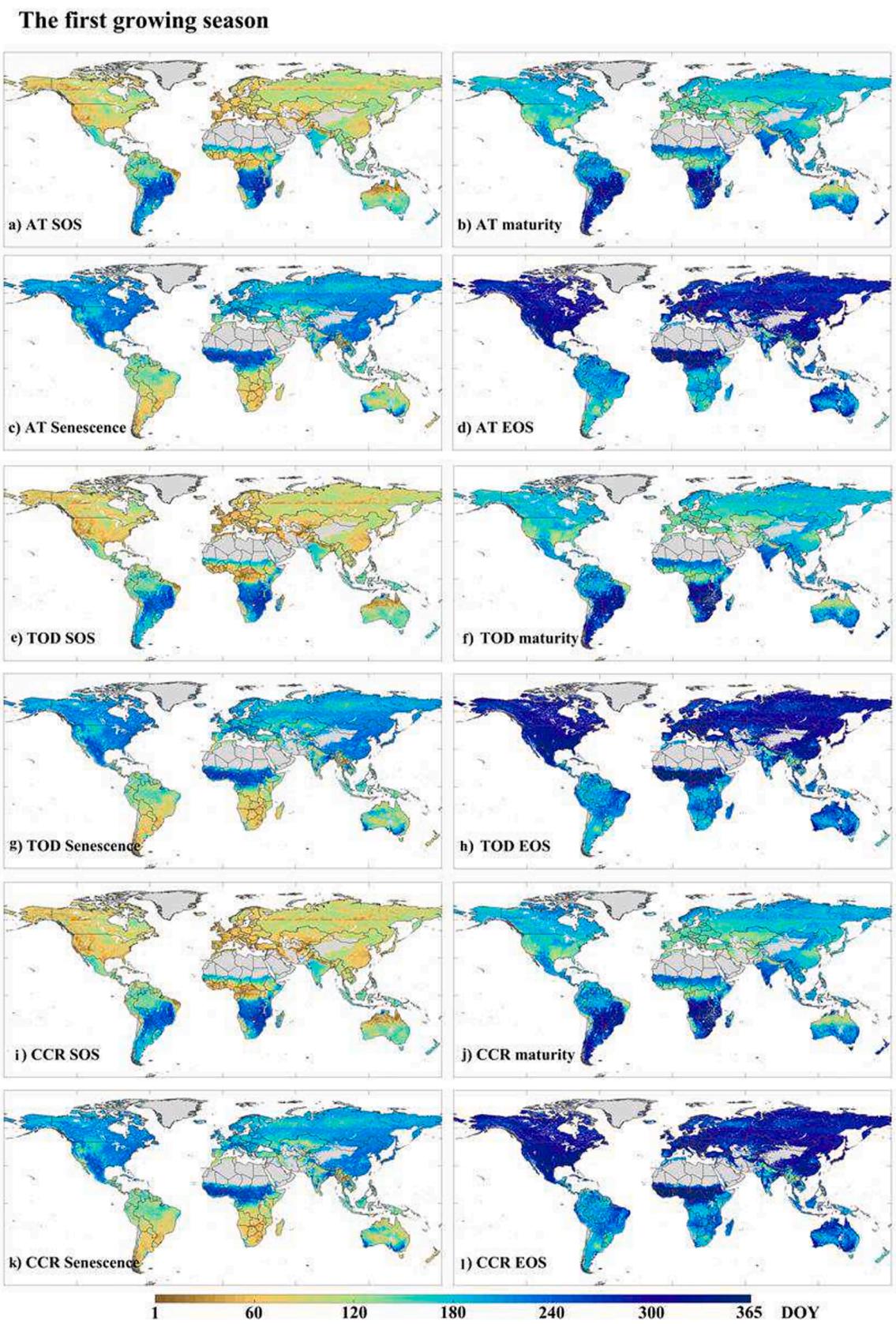

Fig. A1. Distribution of global mean SOS, maturity, senescence and EOS (during the first vegetation growing season of each year) over 37 years (1982–2018) retrieved using AT, TOD and CCR.

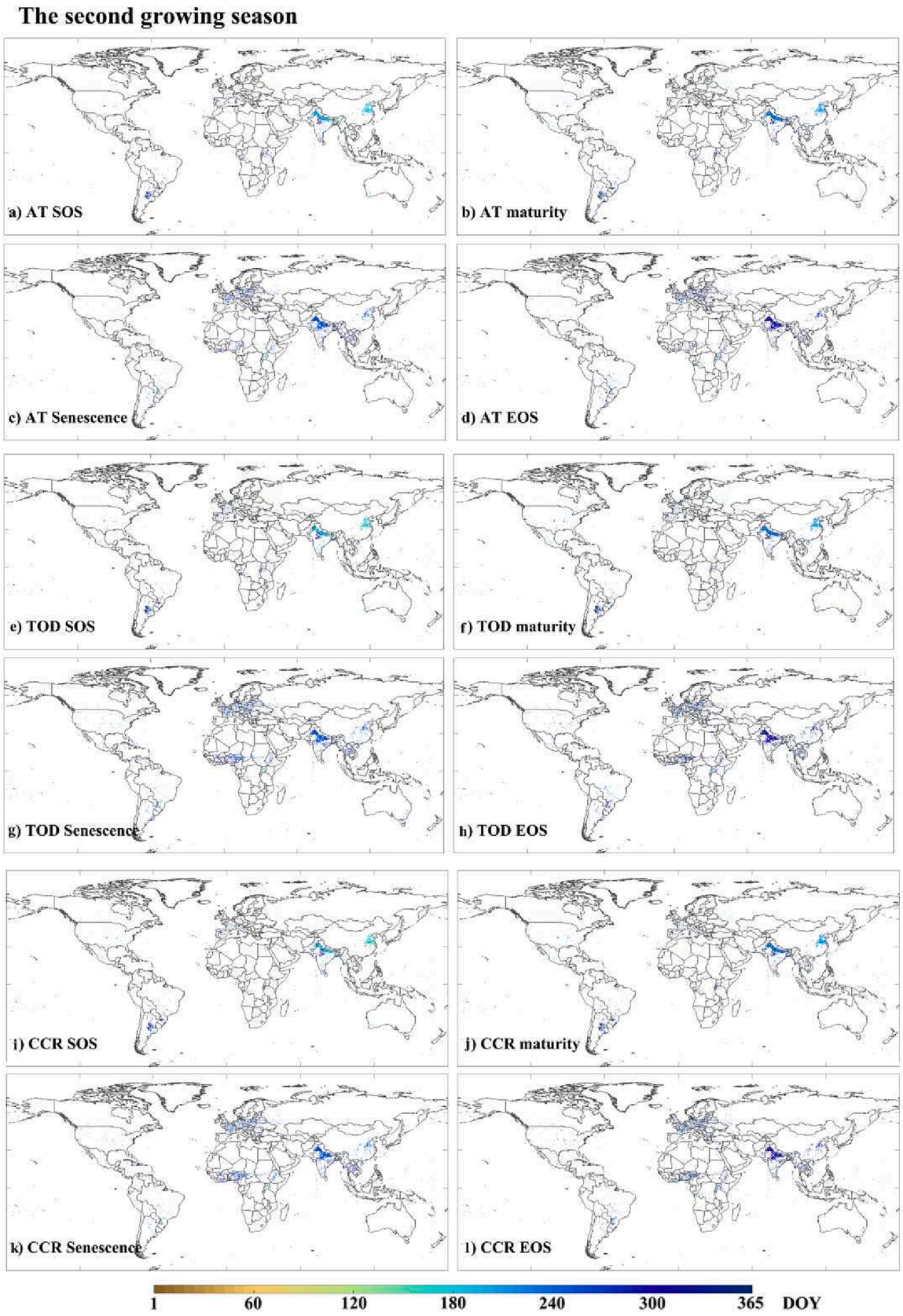

Fig. A2. Distribution of global SOS, maturity, senescence and EOS retrieved using AT, TOD and CCR in the second vegetation growing season of 2015.

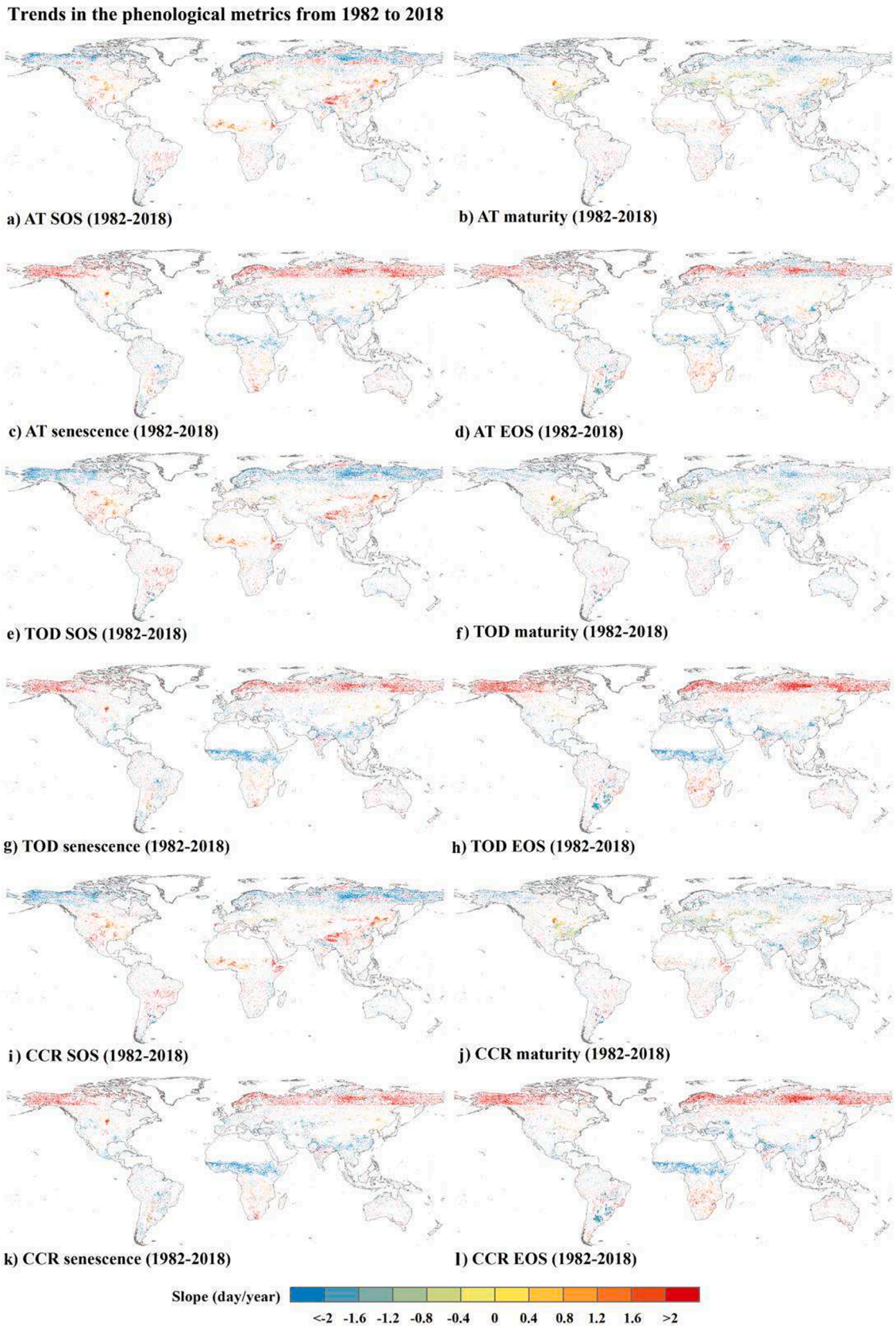

Fig. A3. Trends in the phenological metrics (i.e., SOS, maturity, senescence and EOS) retrieved from the AVHRR data using AT, TOD and CCR from 1982 to 2018.

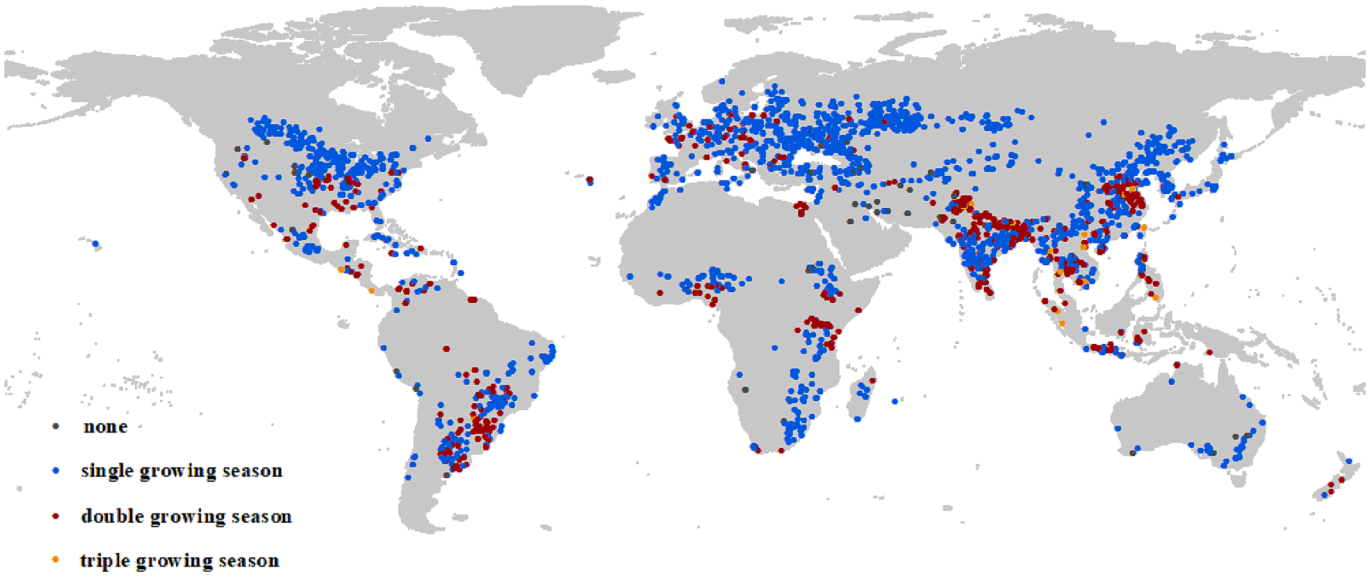

Fig. A4. Global cropping intensity validation sample sites in 2001, for example.

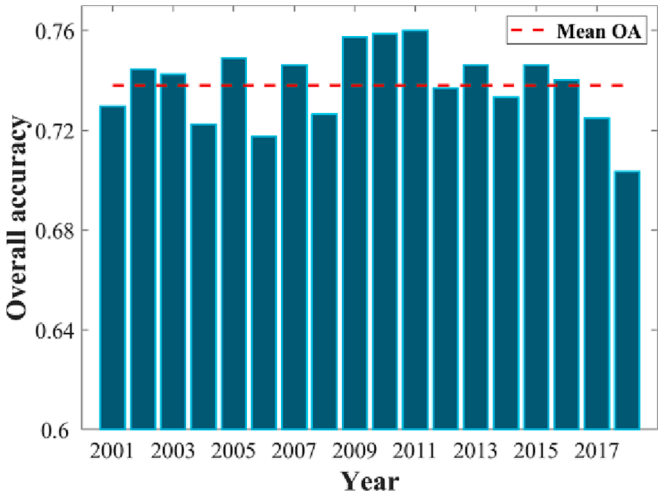

Fig. A5. Overall accuracy of the annual number of vegetation growing season from 2001 to 2018.

the timing of AVHRR-senescence is concentrated in the first half of the year, while the timing of MODIS-senescence is concentrated in the second half of the year (Fig. 3). As vegetation growth in Indochina Peninsula is driven by precipitation and the rainy season of the year is concentrated from May to November (Suepa et al., 2016), vegetation brown-down phase generally lasts from the end of the previous year to the beginning of the rainy season in the current year. According to the statistical principle of vegetation growing season in this study, we identified the vegetation brown-down phase in the region from the end of the previous year as the growth cycle in the current year. In contrast, the brown-down phase extracted by MCD12Q2 in the region started in the winter of the current year and lasted until the next year. Therefore, there is still a large uncertainty in how to identified the vegetation growth cycle of the precipitation-driven vegetation growth regions in the target year.

To effectively assess the number of vegetation growing seasons extracted in this study, we extracted the number of vegetation growing seasons across the five MODIS tiles (i.e., h10v05, h13v12, h18v03, h25v06, and h27v05) in 2012 based on the 250 m MOD09Q1 product, where the tile of h10v05 is located in the Southeastern United States, the tile of h13v12 is located in Southeastern South America, the tile of h18v03 is located in Northwestern Europe, the tile of h25v06 is mostly located in Northern India, and the tile of h27v05 is located in Northern China. The number of vegetation growing seasons extracted in this study is consistent with MCD12Q2 and Global Cropping Intensity (GCI) (Fig. 9). In h10v05 and h13v12, the double growing season region was the most abundant in GCI, followed by this study, and the least in MCD12Q2. In h18v03 and h25v06, the double growing season regions extracted in this study remained consistent with GCI, and were slightly less MCD12Q2. In h27v05, the three products extracted approximately the same double growing season regions, but GCI identified larger triple growing season regions. One possible reason is that the GCI data used an 18-month EVI time series (e.g., the 2012 GCI was extracted from continuous EVI time series from October 2011 to March 2013) to identify the number of vegetation growth cycles per year. Moreover, Fig. A5 shows the annual overall accuracy of the number of global vegetation growing season assessed using the annual worldwide cropping intensity validation samples (Fig. A4) from 2001 to 2018, with the highest overall accuracy of 0.7599 in 2011. Meanwhile, the average overall accuracy from 2001 to 2018 is 0.7381 with a standard deviation of 0.0152. Note that higher accuracy for higher spatial resolution products based on the same validation data. For example, Liu et al. (2021) found that the cropping intensity dataset (250 m) from 2001 to 2019 had a good overall accuracy performance, with an average OA of 88.97% and a maximum precision of 89.97%.

Long-term trends in phenological metrics can reflect the characteristics of climate change. As shown in Fig. 5, in the Northern Hemisphere, both mean SOS and EOS extracted using the four methods (i.e., AT, SOD, TOD, and CCR) did not change significantly from 1982 to 2018; mean maturity extracted using AT and TOD showed significantly advanced trends over the past 37 years; mean senescence extracted using AT, TOD and CCR showed significantly advanced trends between 1982 and 2018. In the Southern Hemisphere, mean SOS extracted using all four methods showed significantly delayed trends from 1982 to 2018, while other phenological metrics exhibited insignificant changes. In other words, this study found that from the 1980 to 2018, summer and autumn were significantly advanced in the Northern Hemisphere and spring was significantly delayed in the Southern Hemisphere. Additionally, the spatial distribution characteristics of the temporal trends extracted using various methods were similar at the pixel scale (Figs. 6 and A3).

The data from different satellite sensors are inherently different, and there are non-negligible spatial scale effects in the phenological metrics

extracted based on different satellite data. At the site-scale, despite that the overall intra-annual trends of the AVHRR-EVI2, MODIS-EVI2, and Fused-EVI2 time series curves are consistent, the time series trajectories from different sensors and the relative magnitude of the EVI2 values are uncertain (Fig. 7). The phenological metrics derived based on the site-scale AVHRR-EVI2, MODIS-EVI2 and Fused-EVI2 time series are relatively close to each other, with a minimum difference of 1 day and a maximum difference of 25 days. Nevertheless, there are significant differences between ground-based and satellite-based phenological metrics, and phenological metrics based on higher spatial resolution satellite data are not necessarily closer to those based on field observations. Taking the Willow Creek site as an example, SOS retrieved from MODIS data, maturity retrieved from MODIS data, senescence retrieved from AVHRR data, and EOS retrieved from Fused data are the closest to the corresponding metrics extracted from field observations, respectively (Table 4). At the regional-scale, the phenological metrics (i.e., SOS, maturity, senescence and EOS) retrieved based on AVHRR-EVI2, MODIS-EVI2, and Fused-EVI2 time series, respectively, remained consistent in spatial distribution (Fig. 8). Nevertheless, the regional-scale mean phenological metrics results (Table 5) indicate that there are large differences in the satellite-based phenological metrics results at different spatial resolutions, which may affect the analysis of the temporal trends of phenological metrics at regional-scale. It is necessary to further develop land surface phenology datasets with different resolutions and to assess their potential for application in different scenarios.

6. Conclusion

We retrieved the global SOS, maturity, senescence, and EOS from 1982 to 2018 using four common phenology retrieving methods (i.e., AT, SOD, TOD, and CCR) based on long time series of AVHRR observations, and accounting for multiple vegetation growing seasons in a year. From 1982 to 2018, summer and autumn were significantly advanced in the Northern Hemisphere and spring was significantly delayed in the Southern Hemisphere. Phenological metrics retrieved using the four methods are positively correlated with those derived from phenology observation networks and flux tower observations. Despite that the differences in satellite sensors have a significant impact on the phenology retrieval, the phenological metrics retrieved based on AVHRR in this study are consistent with those retrieved based on higher spatial resolution, such as MODIS (500 m) and Landsat-MODIS fusion (30 m) time series, at both site-scale and regional-scale. In summary, the developed dataset includes global SOS, maturity, senescence and EOS of two vegetation growing seasons per year extracted by four methods, aiming to provide a reference for the researches and applications of land surface phenology. The global annual land surface phenology data are available at https://doi.org/10.6084/m9.figshare.20375394.v2.

CRediT authorship contribution statement

Wei Wu: Writing – original draft, Writing – review & editing, Software, Validation, Visualization. **Ziming Li:** Writing – review & editing. **Zhicheng Zhang:** Software, Validation, Visualization. **Chenxi Yan:** Validation, Visualization. **Kun Xiao:** Validation, Visualization. **Yidan Wang:** Validation, Visualization. **Qinchuan Xin:** Conceptualization, Writing – review & editing.

Declaration of Competing Interest

The authors declare that they have no known competing financial interests or personal relationships that could have appeared to influence the work reported in this paper.

Data availability

I have shared the link to my data in the manuscript.

Acknowledgments

This research is supported by National Key R&D Program of China (grant nos. 2017YFA0604300 and 2017YFA0604302), Natural Science Foundation of China (grant nos. U1811464 and 41875122), Guangdong Top Young Talents (grant no. 2017TQ04Z359), Western Talents (grant no. 2018XBYJRC004).

Appendix

References

Chen, T., Bao, A.M., Jiapaer, G., Guo, H., Zheng, G.X., Jiang, L.L., Chang, C., Tuerhanjiang, L., 2019. Disentangling the relative impacts of climate change and human activities on arid and semiarid grasslands in Central Asia during 1982–2015. Sci. Total Environ. 653, 1311–1325.

Chen, Y., Cao, R., Chen, J., Liu, L., Matsushita, B., 2021. A practical approach to reconstruct high-quality Landsat NDVI time-series data by gap filling and the Savitzky-Golay filter. ISPRS J. Photogramm. Remote Sens. 180, 174–190.

Dai, J., Wang, H., Ge, Q., 2014. Characteristics of spring phenological changes in China over the past 50 years. Adv. Meteorol. 2014, 843568.

Donnelly, A., Yu, R., Jones, K., Belitz, M., Li, B., Duffy, K., Zhang, X., Wang, J., Seyednasrollah, B., Gerst, K.L., Li, D., Kaddoura, Y., Zhu, K., Morisette, J., Ramey, C., Smith, K., 2022. Exploring discrepancies between in situ phenology and remotely derived phenometrics at NEON sites. Ecosphere 13, e3912.

Elmore, A.J., Guinn, S.M., Minsley, B.J., Richardson, A.D., 2012. Landscape controls on the timing of spring, autumn, and growing season length in mid-Atlantic forests. Global Change Biol. 18, 656–674.

Fischer, A., 1994. A model for the seasonal variations of vegetation indices in coarse resolution data and its inversion to extract crop parameters. Remote Sens. Environ. 48, 220–230.

Fisher, J.I., Mustard, J.F., Vadeboncoeur, M.A., 2006. Green leaf phenology at Landsat resolution: Scaling from the field to the satellite. Remote Sens. Environ. 100, 265–279.

Gan, L.Q., Cao, X., Chen, X.H., Dong, Q., Cui, X.H., Chen, J., 2020. Comparison of MODIS-based vegetation indices and methods for winter wheat green-up date detection in Huanghuai region of China. Agric. For. Meteorol. 288–289, 108019.

Ge, Q., Wang, H., Rutishauser, T., Dai, J., 2015. Phenological response to climate change in China: a meta-analysis. Global Change Biol. 21, 265–274.

Glynn, P.D., Owen, T.W., 2015. *Review of the USA National Phenology Network*. US Department of the Interior, US Geological Survey.

Gray, J., Sulla-Menashe, D., Friedl, M.A., 2019. User guide to Collection 6 MODIS land cover dynamics (MCD12Q2) product. User Guide 6, 1–8.

Guo, L., Dai, J., Wang, M., Xu, J., Luedeling, E., 2015. Responses of spring phenology in temperate zone trees to climate warming: A case study of apricot flowering in China. Agric. For. Meteorol. 201, 1–7.

Hmimina, G., Dufrene, E., Pontailler, J.Y., Delpierre, N., Aubinet, M., Caquet, B., de Grandcourt, A., Burban, B., Flechard, C., Granier, A., Gross, P., Heinesch, B., Longdoz, B., Moureaux, C., Ourcival, J.M., Rambal, S., Saint Andre, L., Soudani, K., 2013. Evaluation of the potential of MODIS satellite data to predict vegetation phenology in different biomes: An investigation using ground-based NDVI measurements. Remote Sens. Environ. 132, 145–158.

Høgda, K.A., Tommervik, H., Karlsen, S.R., 2013. Trends in the Start of the Growing Season in Fennoscandia 1982–2011. Remote Sens. 5, 4304–4318.

Hufkens, K., Basler, D., Milliman, T., Melaas, E.K., Richardson, A.D., 2018. An integrated phenology modelling framework in R. Methods Ecol. Evol. 9, 1276–1285.

Jiang, Z., Huete, A.R., Didan, K., Miura, T., 2008. Development of a two-band enhanced vegetation index without a blue band. Remote Sens. Environ. 112, 3833–3845.

Joiner, J., Yoshida, Y., Vasilkov, A., Schaefer, K., Jung, M., Guanter, L., Zhang, Y., Garrity, S., Middleton, E.M., Huemmrich, K.F., Gu, L., Marchesini, L.B., 2014. The seasonal cycle of satellite chlorophyll fluorescence observations and its relationship to vegetation phenology and ecosystem atmosphere carbon exchange. Remote Sens. Environ. 152, 375–391.

Jönsson, P., Eklundh, L., 2004. TIMESAT—a program for analyzing time-series of satellite sensor data. Comput. Geosci. 30, 833–845.

Justice, C.O., Townshend, J.R.G., Holben, B.N., Tucker, C.J., 1985. Analysis of the phenology of global vegetation using meteorological satellite data. Int. J. Remote Sens. 6, 1271–1318.

Klosterman, S.T., Hufkens, K., Gray, J.M., Melaas, E., Sonnentag, O., Lavine, I., Mitchell, L., Norman, R., Friedl, M.A., Richardson, A.D., 2014. Evaluating remote sensing of deciduous forest phenology at multiple spatial scales using PhenoCam imagery. Biogeosciences 11, 4305–4320.

Liu, Y., Hill, M.J., Zhang, X., Wang, Z., Richardson, A.D., Hufkens, K., Filippa, G., Baldocchi, D.D., Ma, S., Verfaillie, J., Schaaf, C.B., 2017. Using data from Landsat, MODIS, VIIRS and PhenoCams to monitor the phenology of California oak/grass

savanna and open grassland across spatial scales. Agric. For. Meteorol. 237, 311–325.
Liu, X., Zheng, J., Yu, L., Hao, P., Chen, B., Xin, Q., Fu, H., Gong, P., 2021. Annual dynamic dataset of global cropping intensity from 2001 to 2019. Sci. Data 8, 283.
Meier, U., 1997. BBCH-Monograph: Growth Stages of Mono-and Dicotyledonous Plants. Blackwell Wissenschafts-Verlag, Berlin.
Menzel, A., Sparks, T.H., Estrella, N., Koch, E., Aasa, A., Ahas, R., Alm-KÜBler, K., Bissolli, P., BraslavskÁ, O.G., Briede, A., Chmielewski, F.M., Crepinsek, Z., Curnel, Y., Dahl, Å., Defila, C., Donnelly, A., Filella, Y., Jatczak, K., MÅGe, F., Mestre, A., Nordli, Ø., PeÑUelas, J., Pirinen, P., RemiŠOvÁ, V., Scheifinger, H., Striz, M., Susnik, A., Van Vliet, A.J.H., Wielgolaski, F.-E., Zach, S., Zust, A.N.A., 2006. European phenological response to climate change matches the warming pattern. Global Change Biology 12, 1969–1976.
O'Keefe, J., 2021. Phenology of Woody Species at Harvard Forest since 1990. LTER Network Member Node. https://pasta.lternet.edu/package/metadata/eml/knb-lter-hfr/3/33.
Pedelty, J., Devadiga, S., Masuoka, E., Brown, M., Pinzon, J., Tucker, C., Roy, D., Ju, J., Vermote, E., Prince, S., Nagol, J., Justice, C., Schaaf, C., Liu, J., Privette, J., Pinheiro, A., IEEE, 2007. Generating a Long-term Land Data Record from the AVHRR and MODIS instruments, IGARSS: 2007 IEEE International Geoscience and Remote Sensing Symposium, Vols 1-12: Sensing and Understanding Our Planet, pp. 1021-1024.
Piao, S., Cui, M., Chen, A., Wang, X., Ciais, P., Liu, J., Tang, Y., 2011. Altitude and temperature dependence of change in the spring vegetation green-up date from 1982 to 2006 in the Qinghai-Xizang Plateau. Agric. For. Meteorol. 151, 1599–1608.
Piao, S., Liu, Q., Chen, A., Janssens, I.A., Fu, Y., Dai, J., Liu, L., Lian, X., Shen, M., Zhu, X., 2019. Plant phenology and global climate change: Current progresses and challenges. Global Change Biol. 25, 1922–1940.
Reed, B.C., Brown, J.F., Vanderzee, D., Loveland, T.R., Merchant, J.W., Ohlen, D.O., 1994. Measuring phenological variability from satellite imagery. J. Veg. Sci. 5, 703–714.
Richardson, A.D., Anderson, R.S., Arain, M.A., Barr, A.G., Bohrer, G., Chen, G., Chen, J. M., Ciais, P., Davis, K.J., Desai, A.R., Dietze, M.C., Dragoni, D., Garrity, S.R., Gough, C.M., Grant, R., Hollinger, D.Y., Margolis, H.A., McCaughey, H., Migliavacca, M., Monson, R.K., Munger, J.W., Poulter, B., Raczka, B.M., Ricciuto, D. M., Sahoo, A.K., Schaefer, K., Tian, H., Vargas, R., Verbeeck, H., Xiao, J., Xue, Y., 2012. Terrestrial biosphere models need better representation of vegetation phenology: results from the North American Carbon Program Site Synthesis. Global Change Biol. 18, 566–584.
Sakamoto, T., Yokozawa, M., Toritani, H., Shibayama, M., Ishitsuka, N., Ohno, H., 2005. A crop phenology detection method using time-series MODIS data. Remote Sens. Environ. 96, 366–374.
Savitzky, A., Marcel, JE, 1964. Smoothing and differentiation of data by simplified least squares procedures. Analytical chemistry 36, 1627–1639.
Schwartz, M.D., Ahas, R., Aasa, A., 2006. Onset of spring starting earlier across the Northern Hemisphere. Global Change Biology 12, 343–351.
Seyednasrollah, B., Young, A.M., Hufkens, K., Milliman, T., Friedl, M.A., Frolking, S., Richardson, A.D., 2019. Tracking vegetation phenology across diverse biomes using Version 2.0 of the PhenoCam Dataset. Sci. Data 6, 222.
Soudani, K., le Maire, G., Dufrene, E., Francois, C., Delpierre, N., Ulrich, E., Cecchini, S., 2008. Evaluation of the onset of green-up in temperate deciduous broadleaf forests derived from Moderate Resolution Imaging Spectroradiometer (MODIS) data. Remote Sens. Environ. 112, 2643–2655.
Suepa, T., Qi, J., Lawawirojwong, S., Messina, J.P., 2016. Understanding spatio-temporal variation of vegetation phenology and rainfall seasonality in the monsoon Southeast Asia. Environ. Res. 147, 621–629.
Tan, B., Morisette, J.T., Wolfe, R.E., Gao, F., Ederer, G.A., Nightingale, J., Pedelty, J.A., 2011. An enhanced TIMESAT algorithm for estimating vegetation phenology metrics from MODIS data. IEEE J. Sel. Top. Appl. Earth Obs. Remote Sens. 4, 361–371.
Templ, B., Koch, E., Bolmgren, K., Ungersboeck, M., Paul, A., Scheifinger, H., Rutishauser, T., Busto, M., Chmielewski, F.-M., Hajkova, L., Hodzic, S., Kaspar, F., Pietragalla, B., Romero-Fresneda, R., Tolvanen, A., Vucetic, V., Zimmermann, K., Zust, A., 2018. Pan European Phenological database (PEP725): a single point of access for European data. Int. J. Biometeorol. 62, 1109–1113.
White, M.A., Thornton, P.E., Running, S.W., 1997. A continental phenology model for monitoring vegetation responses to interannual climatic variability. Global Biogeochem. Cycles 11, 217–234.
Wu, C., Peng, D., Soudani, K., Siebicke, L., Gough, C.M., Arain, M.A., Bohrer, G., Lafleur, P.M., Peichl, M., Gonsamo, A., Xu, S., Fang, B., Ge, Q., 2017. Land surface phenology derived from normalized difference vegetation index (NDVI) at global FLUXNET sites. Agric. For. Meteorol. 233, 171–182.
Wu, W., Sun, Y., Xiao, K., Xin, Q., 2021. Development of a global annual land surface phenology dataset for 1982–2018 from the AVHRR data by implementing multiple phenology retrieving methods. Int. J. Appl. Earth Obs. Geoinf. 103, 102487.
Xie, Q., Cleverly, J., Moore, C.E., Ding, Y., Hall, C.C., Ma, X., Brown, L.A., Wang, C., Beringer, J., Prober, S.M., Macfarlane, C., Meyer, W.S., Yin, G., Huete, A., 2022. Land surface phenology retrievals for arid and semi-arid ecosystems. ISPRS J. Photogramm. Remote Sens. 185, 129–145.
Xin, Q., Li, J., Li, Z., Li, Y., Zhou, X., 2020. Evaluations and comparisons of rule-based and machine-learning-based methods to retrieve satellite-based vegetation phenology using MODIS and USA National Phenology Network data. Int. J. Appl. Earth Obs. Geoinf. 93, 102189.
Yan, D., Zhang, X., Nagai, S., Yu, Y., Akitsu, T., Nasahara, K.N., Ide, R., Maeda, T., 2019. Evaluating land surface phenology from the Advanced Himawari Imager using observations from MODIS and the Phenological Eyes Network. Int. J. Appl. Earth Obs. Geoinf. 79, 71–83.
Yu, F.F., Price, K.P., Ellis, J., Shi, P.J., 2003. Response of seasonal vegetation development to climatic variations in eastern central Asia. Remote Sens. Environ. 87, 42–54.
Zeng, H., Jia, G., Forbes, B.C., 2013. Shifts in Arctic phenology in response to climate and anthropogenic factors as detected from multiple satellite time series. Environ. Res. Lett. 8, 035036.
Zhang, X.Y., Friedl, M.A., Schaaf, C.B., Strahler, A.H., Hodges, J.C.F., Gao, F., Reed, B.C., Huete, A., 2003. Monitoring vegetation phenology using MODIS. Remote Sens. Environ. 84, 471–475.
Zhou, D., Zhao, S., Zhang, L., Liu, S., 2016. Remotely sensed assessment of urbanization effects on vegetation phenology in China's 32 major cities. Remote Sens. Environ. 176, 272–281.
Zhu, Z., Bi, J., Pan, Y., Ganguly, S., Anav, A., Xu, L., Samanta, A., Piao, S., Nemani, R.R., Myneni, R.B., 2013. Global Data Sets of Vegetation Leaf Area Index (LAI)3g and Fraction of Photosynthetically Active Radiation (FPAR)3g Derived from Global Inventory Modeling and Mapping Studies (GIMMS) Normalized Difference Vegetation Index (NDVI3g) for the Period 1981 to 2011. Remote Sens. 5, 927–948.